

Master thesis: Design and optimization of the pultrusion process to produce reliable and recyclable wind turbine blades

M.W. Peperkamp s1560166
Master Mechanical Engineering (MS3)
m.w.peperkamp@alumnus.utwente.nl

*University of Twente
Supervisor: I. Baran
September 20, 2021*

ABSTRACT: Renewable energy production in Europe consisted for 65.3% of wind energy in 2017[1]. Wind turbine blades are currently made from thermoset composites. The end of life of these blades is 20 to 30 years[2]. Nevertheless they are often already replaced a lot sooner, due to high erosion and better designs being available. The waste from these thermoset blades poses a great environmental problem[3]. The thermoset blades can hardly be recycled, due to the chemical bonds being too strong to be easily broken down or reformed. If a suitable thermoplastic alternative is found, recycling will become much more viable. Due to thermoplastics being easily remelted and remolded. Elium[®] has the potential to be this suitable thermoplastic, it's low viscosity allows it to be used in thermoset production lines, while it's mechanical properties can compete with the current thermoset resins. This research will focus on optimizing the pultrusion process for carbon Elium[®] composites, to enable the production of recyclable spar caps. In this thesis potential improvements to the setup were researched, after which the process variables were studied. The setup has been improved by the addition of a die entrance cooler to prevent resin solidification at the die entrance, and a winch to increase the ease and safety of starting up the production process. The die was improved by incorporating a more robust clamping system. After the improvements, samples of carbon Elium[®] have been successfully produced. These samples have been subjected to 3 point-bending, nano-indentation and microscopy testing. The flexural modulus and strength were found to be comparable to the values published in literature focusing on thermoplastic pultrusion and promising to reach market quality with some process improvements. There existed internal voids and micro scale cracks in the pultruded samples which varied with the change in pultrusion speed and heater temperatures. The hardness test done using nano-indentation showed means around the expected values for a fully polymerised Elium[®]. Recommendations are made for the future of this research, including the switch to a 2-part die and a better pulling unit.

Key words: Composites, Thermoplastics, Pultrusion, Elium[®], nano-indentation, 3-point bending, carbon fiber, resin bath pultrusion

CONTENTS

1	Introduction	3
1.1	Theory	3
1.2	Research goals	6
2	Background	8
3	Die entrance flow model	13
3.1	Iteration 1	13
3.2	Iteration 4	13
3.3	Model validation	14
3.4	Viscosity and die entrance pressure	14
4	Pultrusion line at the University of Twente (UT)	17
4.1	Pulling the fibers	17
4.2	Die entrance temperature	19
4.3	Increase of clamping force	21
5	Experimental	22
5.1	Differential scanning calorimetry (DSC)	22
5.2	Productions	22
5.3	Microscopy	23
5.4	3-point bending test	23
5.5	Nano-indentation	24
6	Results and discussion	26
6.1	Pulling force	27
6.2	Microscopy	29
6.3	3 Point bending	33
6.4	Hardness	35
7	Conclusion	37
8	Recommendations	39
9	Appendix A: Preliminary tests	44
10	Appendix B: Hardness force indentation graphs	47

1 INTRODUCTION

In 2017 65.3% of renewable energy came from wind turbines[1]. The blades of these turbines are made from thermoset composites. The end of life of these blades is 20 to 30 years[2]. From a data set of turbines in Germany however a mean lifetime of only 17.08 years was found[4]. The premature replacements are most likely due to high erosion and better, more efficient, designs being available. These fiber reinforced thermoset composite blades are barely recyclable, due to the chemical bonds being too strong to be easily broken down or reformed. The waste from these blades poses a significant environmental problem, whereas the goal of the wind turbines is to reduce this problem[3]. For example, in the case of wind turbines in the US an estimation is made that for each megawatt of installed production 9.6 metric tons of composite waste is produced[5], similarly 9.7 metric tons is estimated within the EU by Sommers et al.[4], of which 2% is estimated to be carbon fiber reinforced polymer (CFRP) waste. Lefeuvre et al.[6] estimated this to result in over 500 thousand tons of CFRP waste alone by 2050 (see figure 1).

By using thermoplastic composites instead a large part of this waste can be recycled, by remelting and remolding. The switch to thermoplastic composites has been quite slow due to challenges in the production processes. A relatively new thermoplastic resin produced by Arkema has potential to increase the transition speed. The resin called Elium[®] has mechanical and chemical properties close to those of thermoset resins, such as epoxy and polyester. It

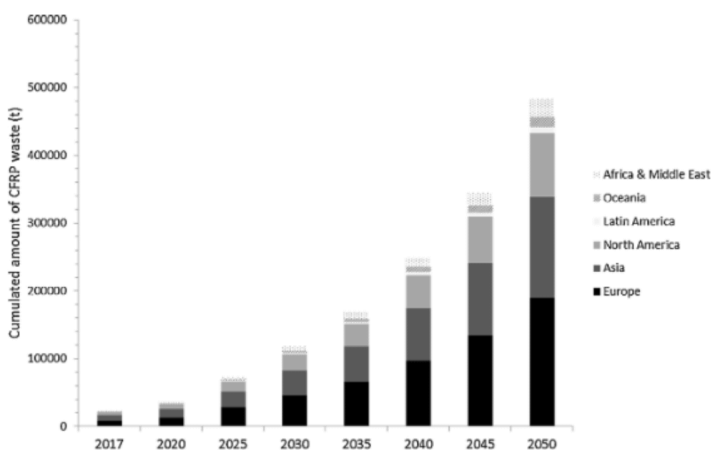


Figure 1: Estimated amount of CFRP waste by geographical area in 2017, 2020 and 2025 [6]

also has a low viscosity which allows it to be used in most thermoset production setups. Elium[®] has already been used in the production of a 9m windmill blade as a test in collaboration with the producer Arkema[7].

An important part of the turbine blade are spar caps (see figure 2). These spar caps are placed over the entire length of a blade and provide it with most of its strength and stiffness. These spar caps experience high tensile and compressive stresses, but only in a single direction. This makes unidirectional composites an ideal material for spar caps, since they have very large a stiffness and strength in the fiber direction, while having a relatively low weight. Currently these spar caps are made from pultruded carbon or glass fibers in combination with a thermoset. In this research the use of Elium[®] for pultrusion will be researched, which could lead to the production of spar caps from Elium[®]. In this way allowing for even better recycleability of the blades.

1.1 Theory

To research this first an understanding is needed of the relevant materials and processes. What is a unidirectional fiber reinforced polymer, how can it be made, why is it perfect to be used for spar caps, why do we want a thermoplastic and which challenges does that bring?

Elium[®]:

Elium[®] is a relatively new material developed by Arkema. The material is made using Methyl methacrylate (MMA), acrylic co-polymers and dimethacrylate ester. It is a thermoplastic resin, but with a low viscosity both before polymerization and above its melting temperature. This allows it to be used in most thermoset pultrusion lines. It has also been proven to have mechanical properties close to and in some cases, impact resistance for example, even better than thermoset alternatives. [9] [10] [11]

Elium is a resin suitable for in-situ polymerization, due to its low viscosity before polymerization, and its suitability for polymerization at room temperature. The process is initialized by the thermal degradation of the peroxides. Once the process is initialized the heat generated by the process itself

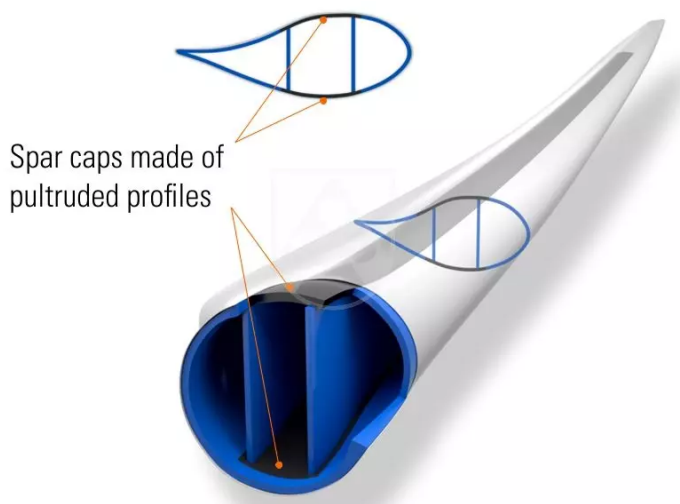


Figure 2: Spar cap in a wind turbine blade [8]

is sufficient to keep the process going. Zoller et al.[12] used this in combination with the solvent cage effect to model this process. In this model, before the reactant can react with other molecules it first needs to diffuse out of its solvent cage. The solvent in this case evaporates allowing the reactant to react with the monomer. This evaporating is highly influenced by the viscosity. A higher viscosity means a stronger cage. The change in viscosity during the conversion results in an efficiency drop between 70% and 80%. Besides the viscosity, the airflow and temperature also play a big role in the speed of evaporation. Zoller et al.[12] used a PREDICI simulation to determine the optimal temperature profile for the combination of peroxides used in that research.

The polymerization of Elium[®] process depends on the types and amount of initiators used. Zoller et al.[12] used a combination of three initiators, a starter, a follow-up and a finisher peroxide [12]. Raponi et al.[13] mentioned differences in the heat flux, total heat and speed, depend on the amount of initiator used. In general a faster polymerization is expected when a larger amount of initiator is used. According to the research of Raponi et al.[13] this is not always true, due to a combination of variables. Therefore care must be taken when deciding the proper amount of initiator.

Before polymerization Elium[®] has a boiling temperature of 100°C. If this temperature is reached before the gelification, bubbles are formed which significantly increase the porosity. To prevent this

from happening during the pultrusion a starting temperature below 100 °C is recommended.

A useful property of Elium[®] is that it retains its properties after having been deformed above its glass temperature. This allows for reshaping and surface texturing after production, without damaging the material.

In research[14] into the pultrusion of polymethyl methacrylate (PMMA), considering that Elium[®] is a variant of PMMA, the results of this are valuable to this research. In their paper [14] they found that in general a lower pulling speed and lower die temperature are beneficial for the mechanical properties. They've set lower limits on these based on the industry. Being a temperature of 140°C and a speed of 400 mm/s. And upper limits, based on thermal degradation of the material and practicality, being 180°C and 1000 m/s. There is also a close relation between speed and temperature, the higher the speed the higher the temperature can and must be, otherwise the material will not be polymerised completely. And the other way around with lower speeds the temperature must be lowered, otherwise the material might degrade.

Pultrusion:

Pultrusion is a continuous production method used to produce long parts with a constant cross-section. The method works by pulling the material through an, often heated, die. The process is very similar to extrusion, in which material is pushed through a die instead of pulled. Pultrusion is especially convenient for fiber reinforced polymers (FRP's). This is due to the presence of fibers, which are also strong while the material as a whole is still in its soft form.

Pultruded products commonly have a specific set of flaws such as porosity, fiber waviness, matrix cracks, or areas of resin richness or starvation [15]. Though the process of pultrusion also results in a high fiber content, about 70wt% and increased mechanical properties due to the tension on the fibers[16].

Thermoset pultrusion:

The most common used matrix type in FRP pultrusion is thermoset. These types of plastic have a low viscosity before curing, which makes it easy to get a good wetting of the fibers. Two common examples

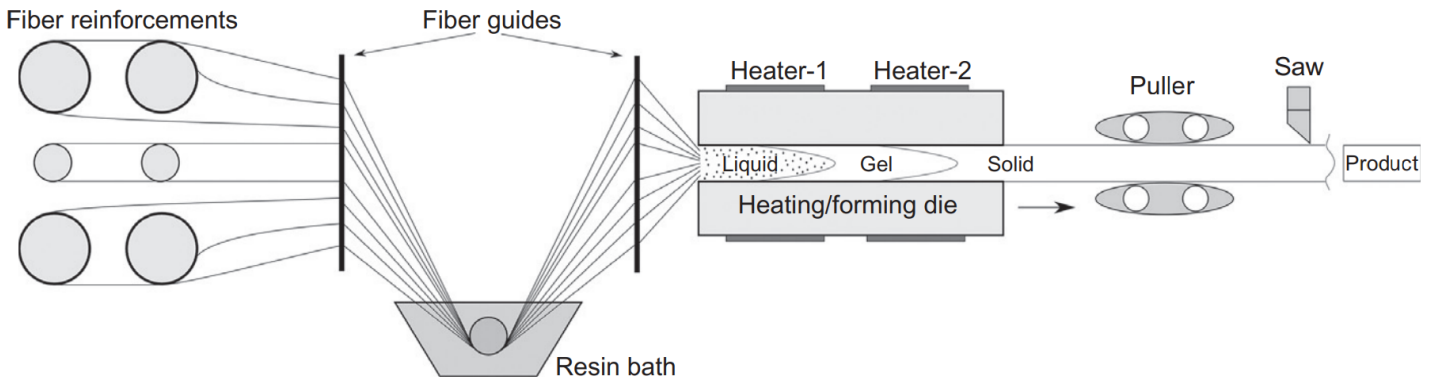


Figure 3: Thermoset resin bath pultrusion line [17]

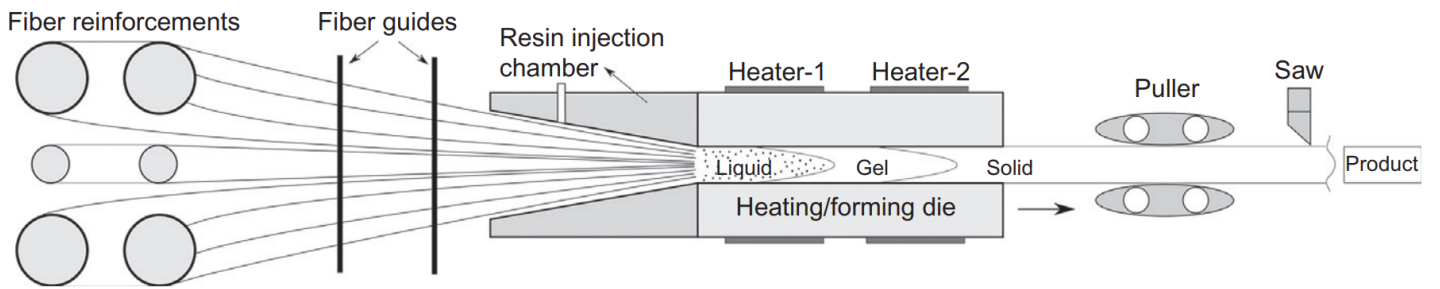


Figure 4: Thermoset resin injection pultrusion line [17]

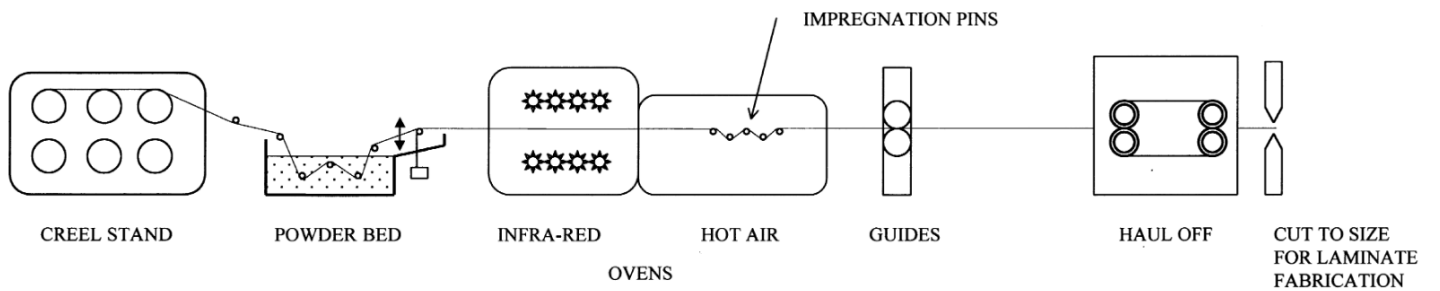


Figure 5: Dry powder impregnation line [18]

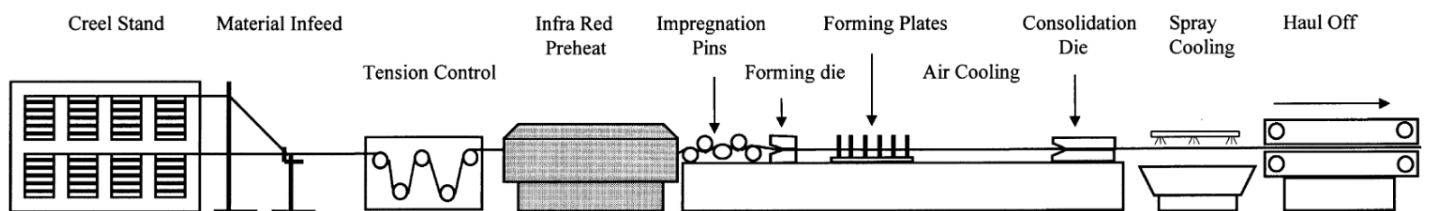


Figure 6: Commingled pultrusion line [18]

of thermoset pultrusion lines are shown in figure 3 and 4. The first one being a resin bath pultrusion line. In this process the fibers are pulled from bobbins through a resin bath. The resin saturated fibers are then pulled through a shape preformer, which leads to the heated die. In this die the material is cured while being in the desired shape. Behind the die, the puller is located, which pulls the material through the entire line. After the puller the material is cut at its desired length. The second option is a resin injection pultrusion line. In this process the resin is injected into the fiber bundles in a resin injection chamber. The rest of the process is the same as in the resin bath process.

Pultrusion using a resin bath has some requirements as mentioned in [12]. Firstly, a high reactivity is needed with a full polymerization time of less than 2 minutes. This is needed to keep the process going at a high enough speed. Secondly, a long pot life is needed in the resin bath. Either 8 hours or the duration of one shift at room temperature, to prevent degradation of the material. Lastly a good wettability of the fiber is needed.

Pultrusion using resin injection, has several advantages over the resin bath system. It allows for better wetting of the fibers, which results in better mechanical properties of the composite. There is less waste resin left in the machine after use. And less solvent is needed in the cleaning after use[19]. The machine is however a lot more complex, which increases the costs and the chance of issues. This process has also been modelled by S.Kouba et al. [20] for thermoplastic use. In that research, the process using thermoplastics was deemed too slow, this study however did not take new lower viscosity thermoplastics into account. K.Chen et al.[21] in 2019 made a resin injection pultrusion line, specifically to be used with a low viscosity nylon 6 (Pa-6). With this machine they were able to make thermoplastic pultruded profiles with a fiber content of 70 wt%.

Thermoplastic pultrusion:

Thermoplastic pultrusion is more complicated than thermoset pultrusion. This is mainly due to the higher viscosity which makes it hard to get a good wetting of the fibers. There are two main ways of dealing with this issue. The first is dry powder impregnation (see figure 5). In this process the fibers are pulled

through a bed of thermoplastic powder. This powder is then melted in a set of ovens. If a good dispersion of powder between the fibers is maintained, then it is a lot easier for the liquid thermoplastic to cover all the fibers. The second technique is commingled (see figure 6). In this process threads of thermoplastic are mixed with the fibers. This mix is then heated in an oven, which causes the thermoplastic threads to melt and wet the fibers.

1.2 Research goals

This research is part of an ongoing research with the end goal being to replace the currently hard to recycle thermoset spar caps with recyclable carbon Elium[®] spar caps. The first step for this is to successfully pultrude carbon Elium[®] samples. This has never been done before and therefore comes with its own challenges. Which include the limited knowledge of what is happening to the Elium[®] in the die and which effect the addition of carbon fibers has on this.

The main goal of this research is "To gain fundamental understanding on the processibility of carbon fiber reinforced Elium[®] composites manufactured by the pultrusion process". This will pave the road to optimize the manufacturing process and to develop in-line process control strategies for maximizing the pultruded products' mechanical performance in the future.

From preliminary research it is known that the die entrance temperature poses an issue, and thus requires investigation. In pultrusion there is a strong relation between the die temperatures and the pulling speed, for this reason the pulling speed is a second point of interest for this research. It is known that both the pulling speed and die temperatures have an influence on the polymerisation, the effect of these two aspects on the polymerisation grade will be a subject in this research. From the reaction of Elium[®] and from previous experiences it is known that gasses are released during the polymerization. This in combination with the difficulty of getting a good wetting in thermoplastic pultrusion, makes the micro-structure an interesting subject of research.

To decide on whether the material produced on this setup is indeed suitable to be used for spar caps, two

other subjects are introduced. The first being, whether it is possible to have a continuous process. Spar caps are very long, spanning the entire length of the blade, the longest ones currently being just over 100 meter long. To produce these a continuous process is a must. For the production process observations are taken into account. Secondly the mechanical properties need to be at least close to the spar caps currently on the market, for it to be viable.

The subjects of research are summarized in the following objectives for this research:

- To investigate the evolution of pulling force during the pultrusion process.
- To determine the flexural modulus and strength of the pultruded carbon Elixir[®] composites.
- To describe the final degree of curing by means of hardness measurements.
- To correlate pulling speed and die entrance temperature with the process observations, resulting micro-structure, hardness and mechanical performance.

Chapter 2 of this research provides background into subjects related to this research. In chapter 3 the die entrance flow model is introduced. The 4th chapter describes the pultrusion line used for this research. Chapter 5 introduces the different tests performed on the produced samples. The 5th chapter contains the results and discussion of the tests mentioned in chapter 4. The conclusion is present in chapter 6 and chapter 7 contains recommendations for the continuation of this research.

2 BACKGROUND

In this section background information will be provided on subjects related to this research.

Fiber reinforced polymers (FRP's):

Fiber reinforced polymers are, as the name states, polymers reinforced with fibers. The fibers give the composite its strength and stiffness, whereas the polymer matrix keeps the fibers together and allows for some flexibility. FRP's are becoming more popular as a construction material. Where at first it was reserved for use in aerospace, due to its very high strength to weight ratio, it is now more and more often used in simple appliances as well.

Despite it being a popular material and it being an active research area, a lot is still unknown about the specific properties. The way the composites are made, results in an uncertainty about its properties. The fibers provide a lot of strength in their length direction, but close to none transverse to it. Since producing a composite with the fibers exactly straight is close to impossible, the strength in the desired direction varies per product. This together with the varying environmental condition at the production areas results in many fluctuations in the product quality [22].

FRP's can be divided into several sub-categories, for example the differentiation between Unidirectional (UD) and Multi-directional laminate can be made. Whereas a UD laminate only has fibers in a single direction, a multi-directional laminate has fibers in several directions by combining several UD layers or the usage of woven mats. UD laminates are a good alternative for constructions loaded in pure bending, pure extension and/or compression. Multi-directional laminates can be tweaked to the precise needs of the situation, reducing mass production possibilities but improving applicability. In this research only UD samples will be produced.

Fibers:

Fibers are the part of a composite which provide the strength and stiffness. There are three common types of fibers, carbon, glass and organic. Each with its own benefits and downsides.

The first carbon fibers were produced by Edison in 1879. These fibers were used for electric lamps and were produced by carefully carbonizing cellulose strands. The starting material for this process was bamboo or cotton. From 1963 onward, carbon fibers are made from either polyacrylonitrile (PAN) or pitch (a by product of the refinement of petroleum). The starting material is stretched to get the required structural and molecular orientation. Different heat treatments are then used to carbonize the fibers. A heat treatment at 200-400°C in air is used for oxidation. A treatment at 1000°C in dinitrogen (N₂) is used for carbonisation. For graphite fibers a heat treatment at 1500°C in Argon (Ar) is used for graphitisation [23].

Carbon fibers consists out of basalt planes (see figure 7). These planes have very strong covalent bonds. The van der Waals forces in between the planes are very weak compared to the in-plane bonds. Due to this, the strength of a carbon fiber depends strongly on the orientation of these planes within the fiber (see figure 8). The more the fibers are parallel to the the fiber direction the stronger the fiber is in this direction, but also the weaker it will be in the transverse direction. In reality the planes are not neatly stacked but more folded around each other as in figure 9. During extension these folds are reduced, the effect of which can be approximated by the rotation of the planes.

Carbon fibers can transfer both electricity and heat very well. This is a property which can be useful in some applications. It for example allows for induction welding when they are used in combination

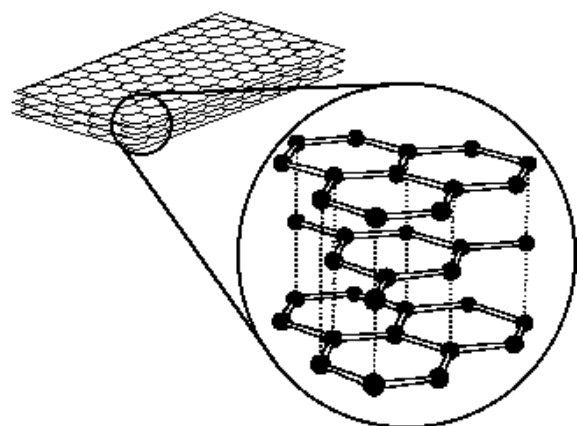


Figure 7: Crystallite structure [24]

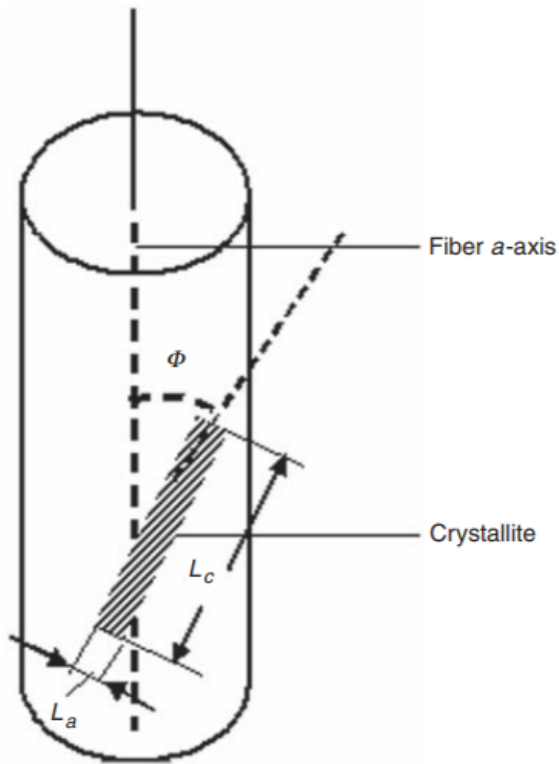


Figure 8: Simplified crystallite orientation within a carbon fiber [24]

with a thermoplastic. For this fibers in more than one direction are needed, such that they together form a closed loop for the eddy currents to flow in.

Carbon fibers are popular due to their high strength and stiffness, their downside is their cost and brittleness. They are commonly used in the high strength parts of planes, cars and wind turbines, but also in hockey sticks for example where a balance is used between carbon and glass fibers. This balance allows the player to choose between a stiff stick for good ball control or a more durable flexible stick.

A slightly cheaper alternative for carbon fibers are glass fibers. Glass fibers are know for the use as fiberglas insulation, fiberglass internet (be it a different form of glass fiber), wind turbines and boats.

Since glass fibers contain few defects and flaws, it is in bulk form stronger than most metals. This makes it a very popular material. Glass fibers are based on silicon-oxides (Si-oxides). The fiber can be tuned for specific purposes by choosing a specific oxide. These Si-oxides are melted at 1300-1500°C (S-glass is melted at higher temperatures). The melted glass then flows through small orifices. It cools down quickly and is pulled at a high velocity (about 65m/s) to produce a fiber. The surface quality with this process is usually below standard, thus a coating is applied consisting of a protective aqueous sizing. This will reduce the effect of any imperfections at the surface [23].

Glass fibers are popular for their relatively low price, their still high strength to weight ratio and their flexibility. Glass fibers are often used as the bulk material for planes and wind turbines.

The least known fibers are organic fibers. An example are Kevlar fibers, which are best known being used in bullet proof vests.

Organic fibers are fibers made from a polymers which are spun to get very thin threads. These threads are then stretched even further to get a high molecular orientation in longitudinal direction which increases the stiffness. This process results in fibers with a very high strength in their longitudinal direction, but very weak in other directions. These fibers have more ductility than carbon fibers and are for this

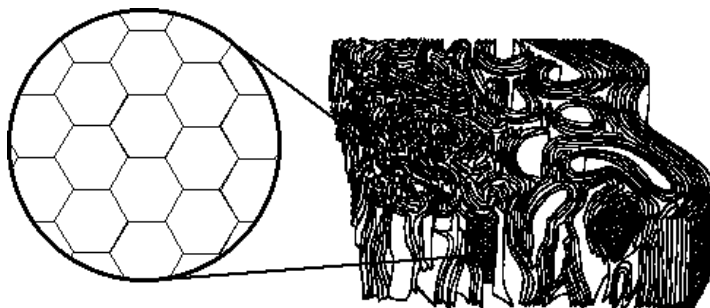


Figure 9: Actual crystallite orientation [25]

reason often mingled with carbon fibers to increase the impact resistance of carbon FRP's [23].

Fiber-matrix interface:

The material consists out of two materials to (theoretically) get the best of both worlds. This does however come with some problems. One of which is that a good bond is needed at the fiber-matrix interface. The material will only be as strong as it's weakest bond, therefore this interface bond needs to have a strength at least close to the strength of the matrix. To do this often a sizing is used on the fibers. This sizing is made of a material which is able to make strong bonds with both the fiber and the matrix. These new interfaces are stronger than the interface would have been without a sizing, thus making it worth to create an extra interface. Besides improving the bond strength it can also work as a protective layer for the fibers against the environment and physical wear.

Carbon fibers have an extra issue when it comes to the interface strength. This issue comes forth out of the structure of carbon fibers. The fibers are made out of basal planes orientated in an angle between 0° - 90° . The strength of these planes are a lot higher than the van der Waals forces between the layers. Due to the production process, the planes on the edge of the fiber are often parallel to the fiber direction. The result is that when the interface is loaded in it's orthogonal direction, the weak van der Waals forces are the limiting factor in the interface strength. This can be prevented by using an oxidation treatment to remove this parallel layer [26].

Voids:

"Regardless of resin type, fibre type and fibre surface treatment, the interlaminar shear strength of composite material decreases by about 7% for each 1% of voids up to a total void content of about 4%. Since other properties are also affected by the presence of voids, it is important to characterize the type of voids and void content." [26]

The reasons for these voids differ per process and material. For most a big reason of voids are the air bubbles in the resin which are created during the mixing of the components. Other resins, Elium[®] for example, go through their boiling point before polymerization. This causes gas to be released during the polymerization. If this gas gets trapped withing

the composite, it forms voids.

Thermoplastic composites:

Thermoplastic composites are composites consisting out of fibers and a thermoplastic matrix. They have several advantages over thermoset composites. Including better recyclability, unlimited shelf life, higher toughness, better moisture resistance and rapid processing [27]. Applications include aircraft parts, cars, bridge decks, window frames, pool floors, cooling towers and much more [28] (See figure 10).

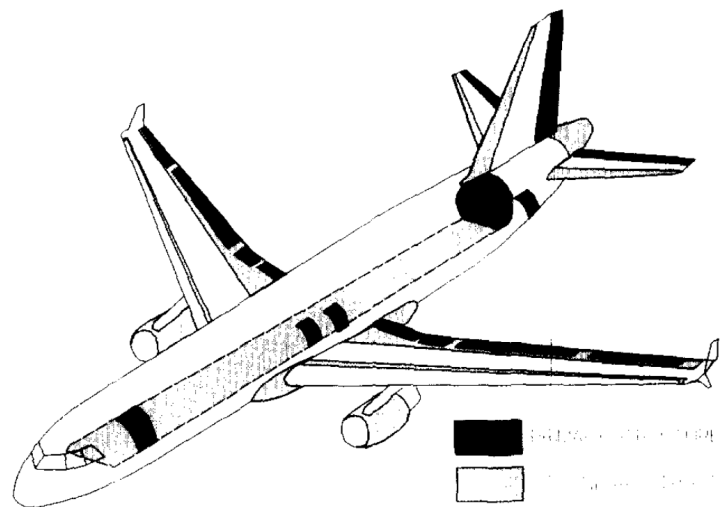


Figure 10: Applications for thermoplastic composites in planes [29]

Forming:

Whereas a thermoset composite after forming cannot be deformed without damaging the material, a thermoplastic composite can be formed and reformed repeatedly if enough heat is applied. This allows for more complicated shapes to be formed than would be possible with a thermoset composite. For example a premade plate of thermoplastic composite can be bought and shaped in a heated mold to get the desired product. Whereas for a thermoset the same product needs to be made in the mold directly. A good example of this kind of product is folding of panel edges using thermofolding. In this process a premade plate or sandwich is folded using a heated die. A technique which can even fold sandwich materials with minimum reduction of material properties [30].

The forming of a thermoplastic composite however has it's downsides. High temperatures are needed to form and deform the thermoplastic. This requires

more energy than the forming of a thermoset composite. Also the viscosity of a liquid thermoplastic is significantly higher than the viscosity of a liquid thermoset. This means that for a good wetting of the fibers higher pressures are needed. Both of these downsides limit the production methods, by requiring more specialized machinery.

Thermoplastics don't always need to be formed with a polymer as a starting point. Some thermoplastics, such as Elium[®], products can also be made by using the monomer as the base material. This usually means a lower viscosity, which allows the material to be used in production methods which are usually reserved to thermosets.

A common application of thermoplastic is fused deposition modeling (FDM), a common technique of additive manufacturing. In this case the possibility to store the virgin material in wire form makes it a very simple process. Upcoming in this field is the addition of chopped fibers to the thermoplastic to increase the stiffness and strength [31]. This could help create stronger and stiffer prototypes. Research is also done into 3D printing with continuous fibers which gives a lot of flexibility in shape and fiber direction, but this is still in an early phase[32].

Another forming processes common to thermoplastic composites is stamp forming. In the case of stamp forming the possibility of re-formability is used to turn a pre-made composite blank into a more complicated form. The blank is heated and then stamped into a die. This process does come with limitations, such as wrinkles in the fibers especially in UD materials [33].

Bonding:

Thermoset composites can only be bonded using a mechanical fastening or an adhesive bonding. Thermoplastic composites have the extra option of being bonded using welding. This has the large benefit of creating a relatively seamless bond. Depending on the fibers used and the direction of those fibers a bond strength close to and sometimes even higher than the strength of the parent material can be achieved [34].

Gohel et al. [35] showed that it is also possible to weld a thermoplastic composite to a thermoset composite if a suitable coating is used. In this research a

carbon/Elium[®] plate was welded to a carbon/epoxy plate with a powdered Elium[®] coating. The tests showed cohesive failure occurred before adhesive failure which is an indication for good bonding.

Failure:

Composites have three major failure modes. The first is failure of the fibers, the second failure of the matrix and the third is failure at the interface between fiber and matrix [27]. Whereas the failure at constant loading is easy to predict, the failure at cyclic loading is still difficult despite a lot of research. It has become clear that failure at a cyclic load is interface and/or matrix determined. Due to this an increased value for the performance was expected with the more ductile thermoplastic matrices over thermoset matrices. Experiments however are inconclusive about this [27].



Figure 11: Playground made from old wind turbine blade parts[36]

Recycling:

Due to the option to remelt thermoplastics, they can be reused in a new product, assuming the material itself has not degraded too much. Compared to the thermoset alternative, which has few options for recycling besides being grounded up and used as road foundation, this is a very large improvement. D.S.Cousins et al.[37] compares several recycling techniques for glass fiber Elium[®] composites to epoxy variants. This research showed that thermoforming, grinding, pyrolysis and dissolution are suitable recycling techniques for Elium[®].

Recently also some more creative options for the

reuse of wind turbine blades have been proposed. For example Bank et al.[38] proposed options for using the blades as roofs for houses and the root sections to lift houses from the ground. In Rotterdam in the Netherlands a playground has been built consisting of old wind turbine blade parts (see figure 11). And in Ireland a pedestrian bridge made from old wind turbine blade parts is being built[39].

3 DIE ENTRANCE FLOW MODEL

To get an estimation of the die entrance pressure built up and to describe the resin backflow in the current die, a model has been made in ANSYS CFX. This model uses the unsteady Navier-Stokes equations in their conservation form. In this model the flow just before and in the first few centimeters of the die has been modelled. In the model the fibers are simulated as a porous medium with a variable porosity with a constant speed. The Elium[®] has been simulated as viscous liquid entering together with the fibers and at the same speed. In this model the fiber volume fraction is increased from 0.3 to 0.7 gradually in the funnel. Before the model was deemed sufficient it went through a total of 4 iterations. In this section the first and last will be discussed in more detail.

3.1 Iteration 1

The first iteration consists of 3 sections (see figure 12), section A is a small startup section, section B is the die funnel and section C is the die cavity. The startup section is used to give excess Elium[®] the chance to leave the domain. This contains excess which enters the model and for the backflow of Elium[®] out of the funnel. The sides of this part are open (atmospheric pressure) for resin to flow out of the domain. The funnel has open sides and free slip walls on the top and bottom at a 45° angle. The die cavity has free slip walls on each side and has an open outlet.

Both the Elium[®] and the fibers entered the model at 3.3mm/sec (roughly 200mm/min), for the fibers this speed was constant where for the Elium[®] the speed after entry was dependent on its interaction with the fibers and the die. In the funnel in this iteration a simple assumption had been made. To get the fibers to flow into the die cavity, the vertical velocity of the fibers was set to be equal to minus the distance to the mid-plane. The horizontal fiber velocity was then calculated using the Pythagoras theorem as to still get a constant fiber speed. This simplification resulted in an overestimation of the vertical velocity and as a consequence an underestimation of the horizontal velocity. A permeability of $3 \cdot 10^{-13} \text{m}^2$ has been used, in practice the permeability is about a factor 10 higher in fiber direction than orthogonal to it, but

considering the limited importance of this model to the research and the work required to implement this properly, only the transverse permeability value is used.

3.2 Iteration 4

A lot of changes have been made from the 1st to the 4th iteration. As a starter the model has been divided into more sections and a section has been added. The new model can be seen in figure 14. Fibers are present in sections A, B and C, sections D and E are located around sections A and B respectively. Section A functions as the start up section similar as in the first iteration. Its main function is still to give the excess of Elium[®] a chance to drip off the fibers and out of the system. Section D has taken over the function of allowing for backflow, this section now does not include any fibers to more closely match the real life situation. Section B is the part of the funnel in which fibers are present. Section E is the part of the funnel where there are no fibers. This section now also includes sides such that the flow of Elium[®] to the sides can also be analysed. Section C is the die cavity. In this iteration the presence of air, by turning the model in a multi-phase flow model, and gravity have been added to the model to give a more realistic representation of the real process.

In figure 14 all walls are shown in transparent blue. All walls present are solid no slip boundaries. The inlet (fluid) consists of 100% Elium[®] with a velocity of 3.3mm/sec. The outlet velocity is now also set to 3.3mm/sec instead of the open boundary from the first iteration. This to simulate the condition that once the Elium[®] becomes solid it will move at the same speed as the fibers. All other sides of the model are 'open' boundaries with 100% air.

The permeability has been updated to the Kozeny-Carman equation in line with "Fluid Mechanics Analysis of a Two-Dimensional Pultrusion Die Inlet" by Sharma et al. [40]. In this equation K_{11} is the permeability in fiber direction, D_f is the fiber diameter, 10 micron in this research, and C is the Kozeny constant which has been chosen to be 1.4. This means that the permeability is now a function of the volume fraction and changes over the length of the model. The fiber velocities in the funnel have

been adjusted to use both the current horizontal and vertical position of the particle in the Pythagoras theorem, resulting in a straight line.

$$K_{11} = \frac{D_f^2(1 - V_f)^3}{(16C)V_f^2} \quad (1)$$

In figures 16 and 17 the resin flow lines can be seen from the side and front respectively. Here it can be seen well that the resin back-flow on the bottom will simply flow down out of the funnel, and from the top the back-flow partially flows down along the sides of the fibers and the rest gets trapped for a while in a circular motion on top of the fibers just before the funnel.

In figure 18 the pressure distribution on the mid-plane can be seen. A high peak can be seen just before the die entrance. The expectation is that this pressure build up plays an important role in the pulling force needed during pultrusion.

3.3 Model validation

The model has been compared to the models in Investigation of the pressure behavior in "a pultrusion die for graphite/epoxy composites" of Raper et al.[41] and "Fluid Mechanics Analysis of a Two-Dimensional Pultrusion Die Inlet" by Sharma et al. [40]. The self made model has been reformed to match the funnel shapes from Raper[41] and Sharma[40], all other settings have been kept the same except for the fiber flow. In the models of Raper[41] and Sharma[40] the fibers don't move with the funnel, but simply go on straight and disappear into the walls of the funnel. To get a similar pressure distribution the same principle has been used in the comparison models. In figures 19 and 20 the pressure distribution in the comparison models has been put next to the pressure distribution from the papers of Raper[41] and Sharma[40]. Here it can be seen that the models match well, especially for the Sharma[40] model. In the Raper[41] comparison there is a mismatch towards the end of the funnel, which could be caused by Raper[41] simulating a longer part of the die cavity. Values of the pressure are deliberately not mentioned for the comparison models, since the exact values for the material properties etc. used in the research are not known, thus only the shape of the

distribution is compared and not the actual values.

3.4 Viscosity and die entrance pressure

Since the premature increase of viscosity at the die entrance has been defined as one of the problem areas, the die entrance pressure dependence on the resin viscosity has been researched in the model. The result can be seen in figure 21. The lowest viscosity in the graph is the viscosity of Elium[®] at room temperature and the highest is a common value for a viscoelastic polymer. Here a clear linear relation is seen between the die entrance pressure and the viscosity of the resin even up to very high viscosity's. Since the die entrance pressure plays a direct part in the pulling force, this signifies the importance of keeping the viscosity of the resin at the die entrance low.

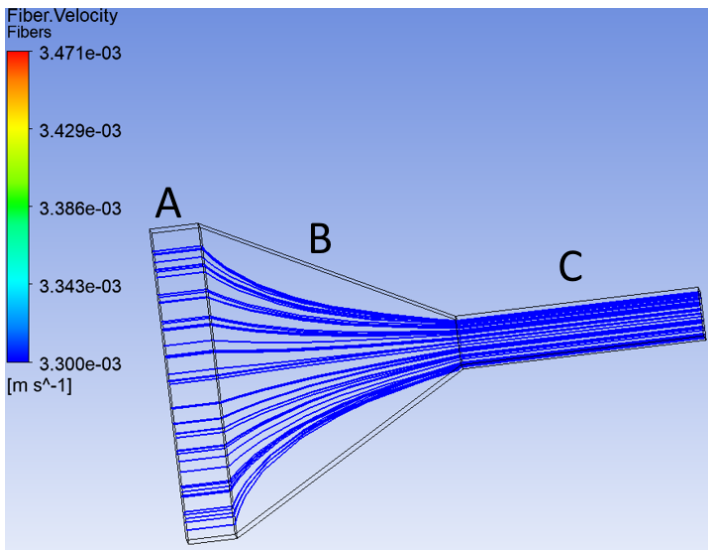


Figure 12: Fiber flow in iteration 1

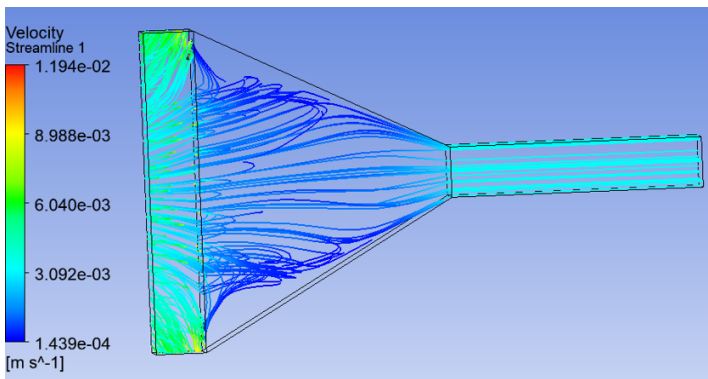


Figure 13: Fiber flow in iteration 1

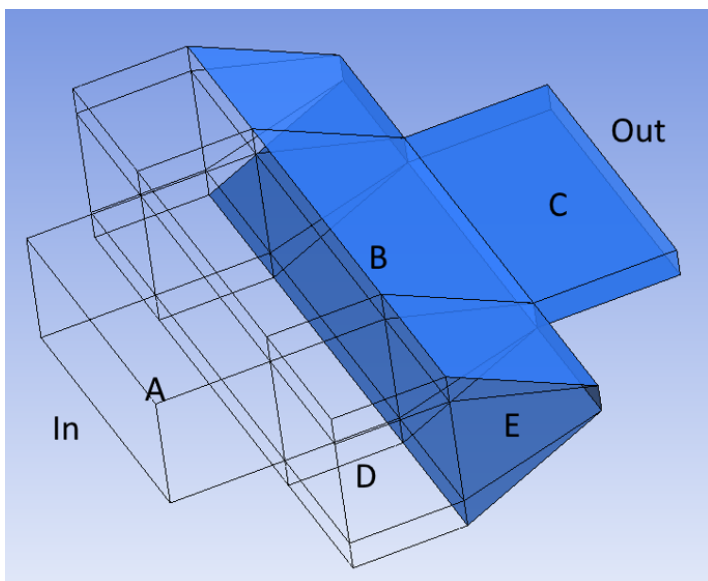


Figure 14: Overview of the 4th iteration of the model

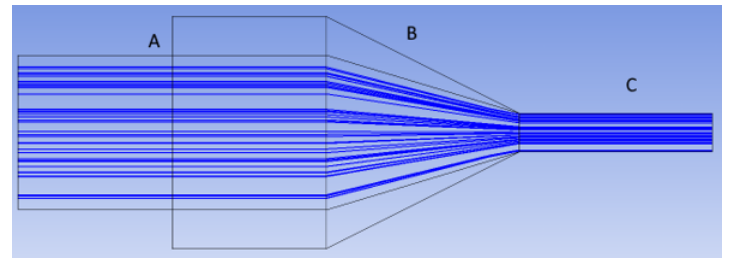


Figure 15: Fiber flow in the 4th iteration of the model

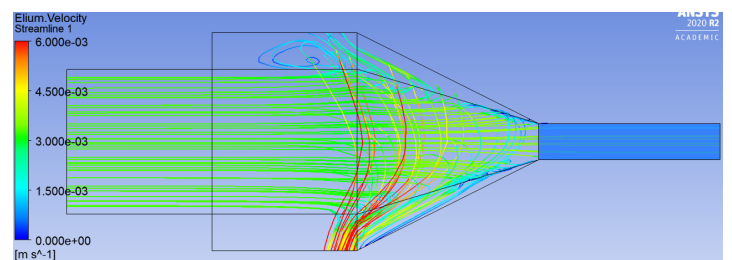


Figure 16: Resin flow in the 4th iteration of the model seen from the side

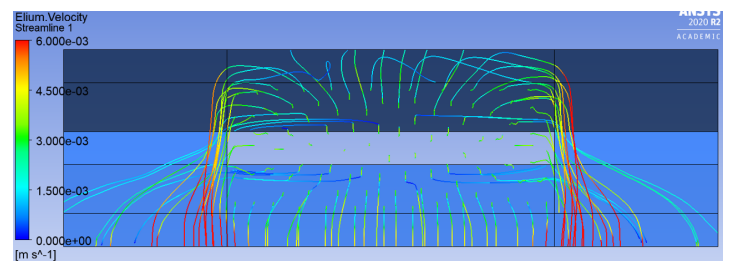


Figure 17: Resin flow in the 4th iteration of the model seen from the front

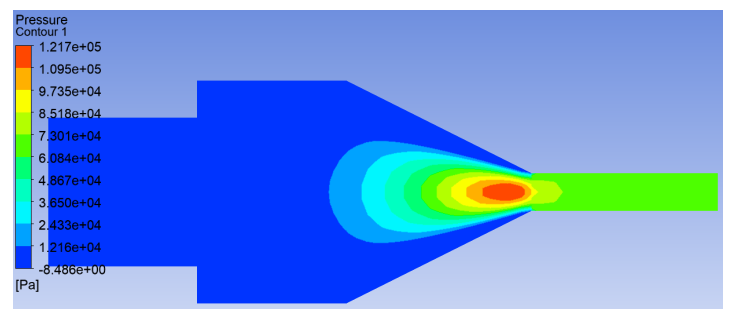


Figure 18: Pressure distribution in the mid-plane of the 4th iteration of the model

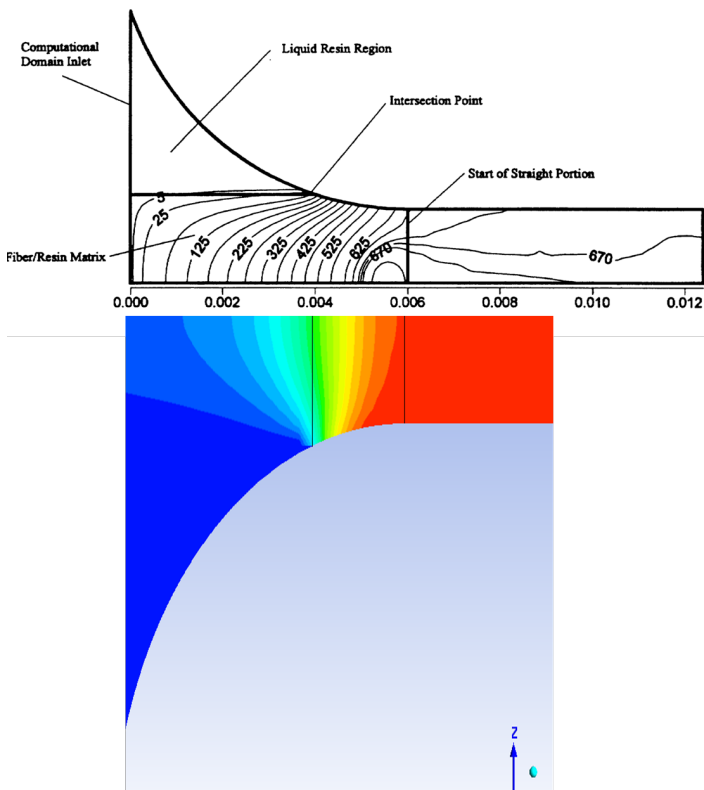


Figure 19: Comparison of pressure fields with the model made by Rapper et al. [41]

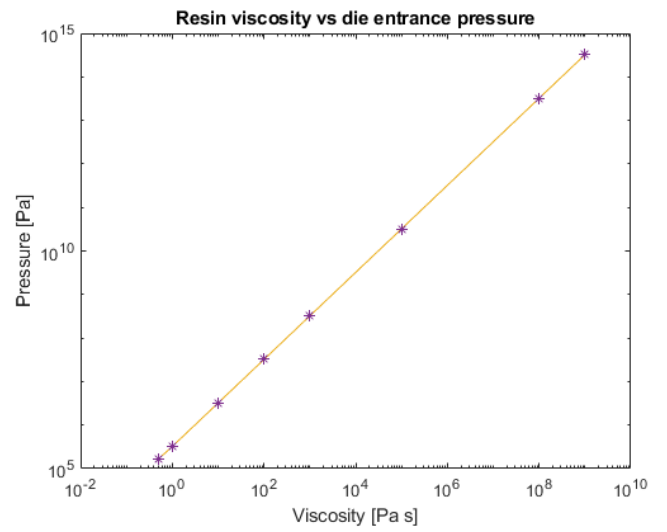


Figure 21: Die entrance pressure vs resin viscosity on a loglog scale

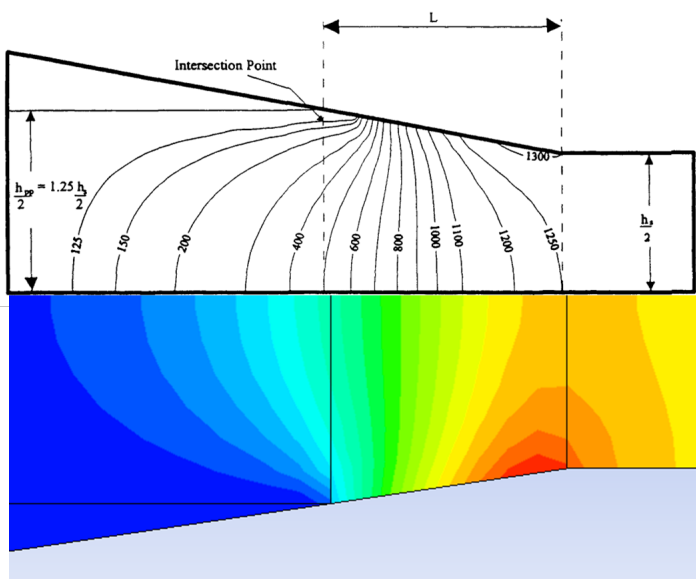


Figure 20: Comparison of pressure fields with the model made by Sharma et al. [40]. Upper half: Sharma, lower half: new model

4 PULTRUSION LINE AT THE UNIVERSITY OF TWENTE (UT)

This research is done on the setup present at the UT designed and build by Jasper van Meurs. The setup can be seen in figure 22. It consists out of bobbin holder, several fiber guides, rollers, a resin bath, 4 heating zones (2 sections having each a top and bottom zone) and a puller consisting of 2 metal rolls actuated by a stepper motor.

The first part of this research is focused on getting this setup to work properly with the carbon Elixir[®] combination. Some problem areas have been defined in preliminary tests (see section 9), being solidification at the die entrance and deformation at the rollers. Two other productions have confirmed the solidification at the die entrance in a more drastic manner. With the temperature in the lab being higher for the second and third productions, the solidification happened even faster. This meant that barely any or no production was possible before the line got stuck (see figure 23). For this reason the optimization is focused on this problem area. The problem of solidification consists out of two sub-problems, being the high force needed to pull the impregnated fibers through the die and the high temperature of the die entrance.

4.1 Pulling the fibers

At the beginning the process there is no polymer product at the rollers. Since the rollers don't have enough grip on the dry fibers, the pulling has to be done by hand until the finished product has reached the rollers. If this does not happen fast enough, the resin at the entrance has already hardened too much to be pulled into the die.

Potential solutions for this issue are adjusting the current puller such that it has grip in the dry fibers or adding a separate puller, automatic or by hand, specifically for the dry fibers. During this phase, negotiations about a new pulling unit were already ongoing, for this reason it was not deemed useful to adjust the current one. Similarly an extra automatic pulling unit would be unnecessary if the new one is already capable of pulling the dry fibers. Therefore a hand powered separate puller was chosen to solve the problem for the duration of this research.

With the choice for a hand puller being made, the design requirements had to be set. In this case a transmission is needed between the force applied by hand and the force applied to the fibers. The concept of a winch (see figure 24) was chosen for this due to its simplicity in both use and production. The winch will consist out of two shafts. The first of which will be placed just behind the original puller, held up by two laser cut plates attached to two aluminum beams. The second shaft slides into a hole in the first shaft. In this way allowing to either use it at full length for maximum transmission or at halfway for ease of turning.

The force needed on the fibers was determined, from the highest force measured during the tests, to be 2kN. With this in mind, and the width of the test setup known to be 200 mm, the required diameter of the main shaft could be determined using equations 2 and 3. This in combination with the available materials in mind, resulted in a steel shaft with diameter of 30mm being chosen as a safe choice. Having a maximum stress of 38MPa well below the 250MPa yield strength of steel. The required diameter of the second shaft can be determined using equations 4 and 5. Based on this a diameter of 20mm was chosen resulting in a maximum stress of 38MPa again well below the yield strength of steel.

$$M_{b1} = \frac{FL_1}{4} \quad (2)$$

$$\sigma_{b1} = \frac{M_{b1}r_1}{I_1} \quad (3)$$

$$M_{t1} = M_{b2} = F * r_1 \quad (4)$$

$$\sigma_{b2} = \frac{M_{b2}r_2}{I_2} \quad (5)$$

With the diameter of the shafts known the transmission ratio could be determined by dividing the length of the second shaft by the diameter of the first. With a convenient length chosen of 500mm this results in a force needed of 60N when the full length is used and

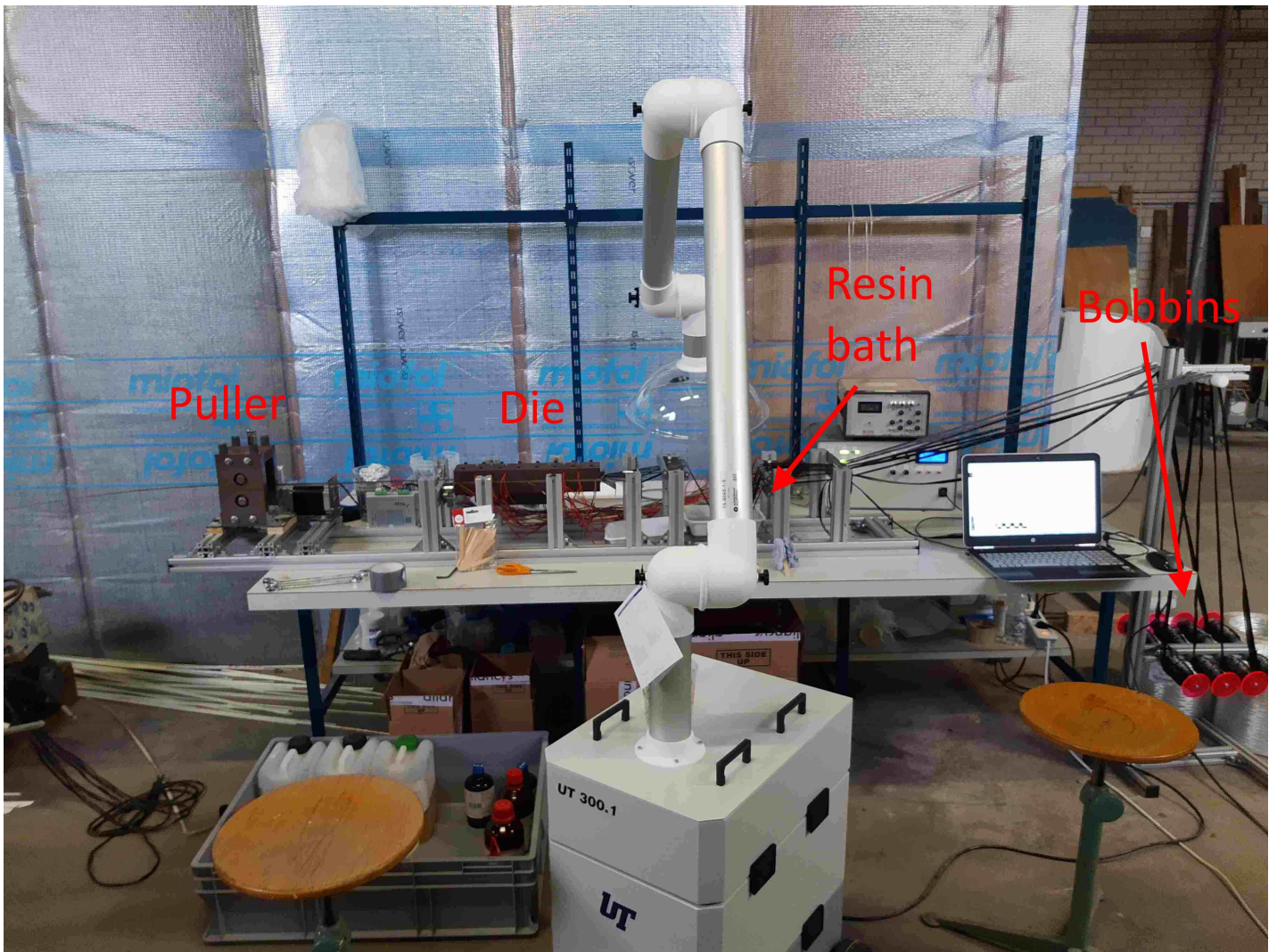


Figure 22: Pultrusion setup



Figure 23: Material stuck in the die entrance



Figure 24: Winch design

120N when the shaft is inserted halfway.

The winch has been installed just behind the puller, this allows for a stiff connection to the rails of the setup. During operation the first few fiber bundles are still pulled by hand, but once this becomes tough the bundles are put through a hole in the winch. After this the bundles will clamp themselves onto the winch and the bundles can easily be pulled further by turning the winch

The winch allows for a more constant speed during the setup of the process. It also significantly reduces the physical work of pulling the fibers. Before the

addition of the winch, if the fibers would snap, the operator would fall backwards with the potential of injuries. The addition of the winch removes this problem, by switching to a turning motion instead of pulling and reducing the required force by roughly a factor 15.

4.2 Die entrance temperature

The temperature at the die entrance has been determined to be 85°Celsius, when the first heating section is set at 90°Celsius. The polymerization of Elium[®], with the thermal initiator used in this research, starts at 50°Celsius. Therefore the die entrance temperature should preferably be lowered to below 50°Celsius. The die entrance temperature also needs to be controllable in order to answer the research objective of identifying its influence on the produced material.

The first attempt to lower this temperature was to elongate the die entrance 10 cm before the heating block. In this way it was managed to drop the temperature to 70°Celsius. This is not enough, especially since the temperature of the heating sections might be increased in future research. There are several options to decrease the temperature even further, three of the options will be discussed.

The first option is a cooling fan. This cools the die entrance by creating a room temperature air flow over the die entrance. This would be done using a fan placed close to the die entrance. Potentially a heat-sink can be added to increase the efficiency of the cooling. Advantages of this concept are that a cooling fan is easy to get your hands on, cheap and the installation requires no changes to the current setup and no coding.

Downsides are that the decrease in temperature is strongly related to the room-temperature in the lab, this would mean that the amount of cooling present is inconsistent between tests and is difficult to control using a standard fan. This would mean the addition of an extra unknown into the variables of this research, which is unwanted since it could influence the reliability of the results. A second downside of creating an airflow is that the polymerization of Elium[®] is based on evaporation which is sped up by an airflow. This could mean that the process which

we want to slow down by the addition of a fan could potentially speed up the process instead. Lastly only the fan speed can be controlled and not the resulting die entrance temperature.

The second option is a Peltier element. This element 'pumps' the heat from the die to the air. Advantages are that it does not create an airflow, is easily connected to the Arduino already present in the setup and that it can be turned on and off easily. This would allow for a feedback loop between the Peltier element and the Arduino, theoretically allowing for a well controllable die entrance temperature.

The efficiency of the Peltier element are however also highly dependent on the room temperature. The amount of heat which can be transferred to the air surrounding the die entrance depends on the difference in temperature between the two. This means that on a hot day the efficiency is lower and also that during the process the efficiency will drop over time, by the air being heated up by the Peltier element itself. This could be improved by the addition of an airflow to transport the heat away from the peltier element, but as mentioned earlier an airflow is not an option.

The third option is a water cooling system, using a thermobath, two aluminum blocks and some heat resistant hoses. The temperature of the cooler can be easily managed by settings of the thermobath which contains a stable cooler. The system is more than strong enough to keep the cooler at a constant temperature during the tests. This option does require a relative large amount of work to install. The blocks of aluminum need to be ordered and milled, the hoses and hositails need to be ordered and installed, the thermobath however is already present at the university.

From these three options the water cooling system has been chosen, for it's reliability and since the relatively high complexity was still quite feasible. A quick model showed that the die entrance would be the same as the water temperature, if the water temperature is assumed to be constant.

The cooling blocks have been kept simple, by using straight holes through an aluminum block. Each hole has thread on both sides such that hose tails can be attached. All 16 (4 holes per block, 2 hose tails per

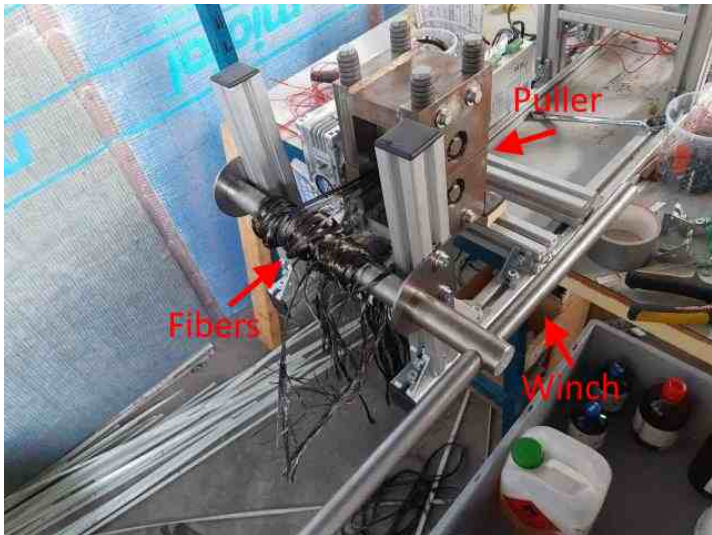


Figure 25: Winch after use

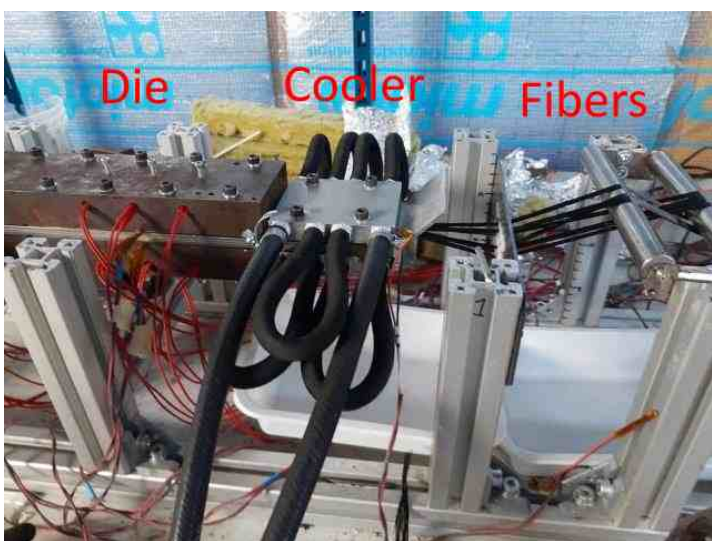


Figure 26: Cooling block in use

hole) are connected to each other and the thermobath using heat resistant tubes. The tubes are connected such that all connections between the blocks are on one side, in this way allowing the blocks to be folded over the die for easy installation. The blocks are clamped to the elongated die using 4 bolts of the same size as used to clamp the heating blocks.

First trials showed that the die entrance indeed had the same temperature as the water (in this case 20°C) and that the resin stayed fully liquid until after the cooler.

4.3 Increase of clamping force

Towards the end of this research the M5 bolts and the thread in the bottom heating block used to clamp the die shut, were worn out. The decision was made to switch to M8 bolts to increase the maximum clamping force, in order to reduce the odds of leakages. The thread in the bottom heating block was replaced by nuts. This allows for more ease in replacing when the thread wears out again. Now only the bolts and nuts need to be replaced.

5 EXPERIMENTAL

With the improved setup finished, the research into the process variables could start. In this section the different tests, their relevance and the related calculations will be discussed.

5.1 Differential scanning calorimetry (DSC)

The DSC test has been performed at 100 degrees Celcius with 1, 2, 3 and 4 weight-percent of peroxide. The results can be seen in figure 27. From this figure it becomes clear that the polymerization is the fastest at 4 weight-percent of peroxide, which will therefore be used for the tests. This results in a polymerization duration of roughly 50 seconds. The conditions in the actual setup will be very different, therefore this value is only an indication and will probably not be the same for the actual productions.

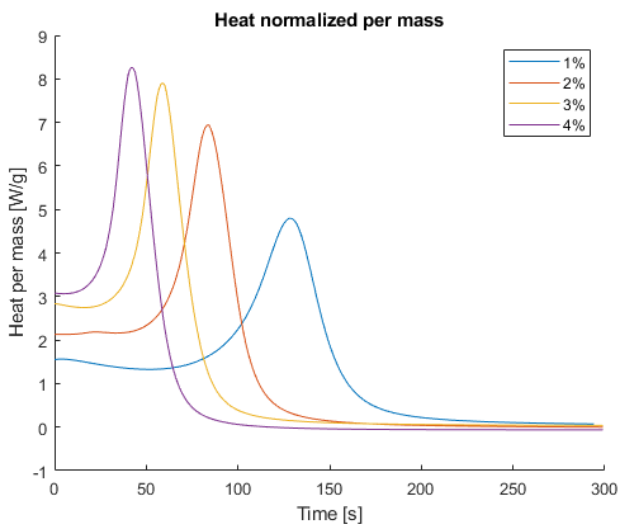


Figure 27: DSC results

5.2 Productions

Producing test samples in it's way is a test on it's own. During the production the temperatures in the heating die and the pulling force are measured. By relating the forces to the different variables used, conclusions can be made about the quality of the process.

The mold itself is located on a sled, which allows for back and forward movements during the process. On the outlet side this movement is limited by a force sensor. Considering that with Newton's third law the

pulling force needed to pull the material through the die should be equal to the force applied to the die, this allows us to measure the pulling force.

During the tests 5 thermocouples are present in the die, 4 are used to control the heating cartridges, in the middle of both heating sections one thermocouple just below and one just above the die cavity, and one at the start of the first heating section. Initially one was also placed at the die entrance, but validation with an external thermocouple showed that the thermocouples used are not accurate at low temperatures. The die entrance is for this reason considered to be the temperature of the thermobath, which has been proven to be a valid assumption with an external thermocouple.

For all productions 6 bundles of carbon fiber have been used in the preform orientation shown in figure 28. Based on the DSC test a initiator content of 4wt% has been chosen for to get a high reactivity. The Elium[®] resin has been mixed with the 4wt% of Perkadox 16 and 1wt% of release agent and stirred carefully until it became a clear mixture.

The die temperatures and pulling speeds for the tests have been decided based on recommendations from Arkema and research from Zoller et al. on Elium[®] pultrusion[12]. From Arkema it is known that the boiling temperature of the monomer is a 100°C and pultrusion temperatures between 65°C and 115°C are recommended. It is preferred to not reach the boiling temperature until the Elium[®] has fully transitioned into it's gell-phase, meaning that

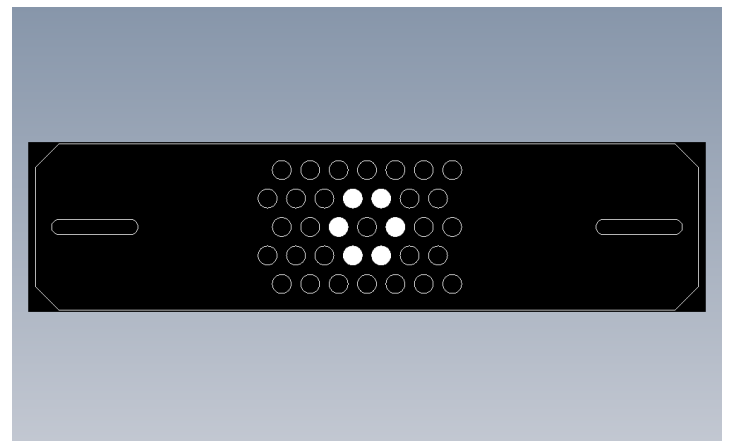


Figure 28: Fiber preform orientation. The holes which are used are shown in white.

the first heating section should be below 100°C. With the recommended max being 115°C and Zoller having performed successful productions in a mold with sections at 90°C and 110°C, it was chosen to in this research also use a 90°C first heating section and a 110°C second heating section.

Knowing the temperatures and having the results of a DSC test at 100°C. The required time in the die is expected to be roughly 60 seconds. With the die having a length of 400mm this results in a maximum speed of 400mm/min. Preliminary tests (see Appendix B) have shown that 400mm/min is too fast but 300mm/min seems to work. With 300mm/min being set at as the max speed, the decision has been made to perform the tests at 100mm/min, 200mm/min and at 300mm/min.

The second variable to be varied is the die entrance cooler temperature. Knowing that the polymerisation of Elium® starts at 50°C, and wanting to stay well below this, the decision has been made to perform tests at 20°C and 40°C. This results in a total of 6 tests to be performed, by combining performing each of the three speeds at both die entrance temperatures.

5.3 Microscopy

From each variable set 2 pieces of approximately 10mm are embedded in epoxy and afterwards polished. These samples are used both for the microscopy inspection and the nano-hardness tests. During the microscopy inspection, an estimation is made of the fiber volume content, the void content and deviations in the micro-structure are noted. Possible deviations are uneven fiber distributions and cracks.

The fiber volume fraction can be determined by doing an image analysis on the microscopy images. This is done according to the "composites material handbook"[42] guidelines. This means that the image is translated to a grey scale on which then a threshold (see figure 29) is determined for the range of grey in which the fibers are present. The volume fraction is then simply calculated by counting the pixels in the threshold and dividing this by the total amount of pixels. This is a quick and easy way to calculate the volume fraction, but the image quality and the threshold settings can influence the results.

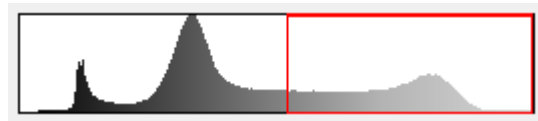


Figure 29: Grey scale threshold for fibers

From the volume fractions the void volume fraction is the most interesting. Voids are pockets of gas in the material. These pockets can decrease the strength of the material significantly by being an easy starting point for cracks. In these productions there will be two potential sources of voids, being air trapped in the resin during mixing or when entering the die and gas released by the resin during polymerization. The air being trapped in the resin can't be controlled during these productions due to the lack of an automatic mixer or a degasser. The amount of gas released by the Elium® is expected to be highly dependent on the speed and temperatures, this will therefore make the void content an important material property to investigate.

The void volume fraction is determined in the same way as the fiber volume fraction, but with a different grey scale threshold (see figure 30).

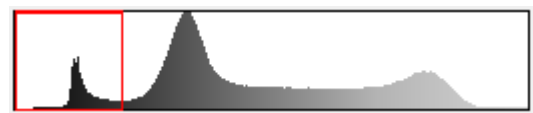


Figure 30: Grey scale threshold for voids

5.4 3-point bending test

To determine the strength and stiffness of the samples a 3-point bending test is performed based on the ASTM "Standard Test Method for Flexural Properties of Polymer Matrix Composite Materials" [43]. In accordance with the standard, per set of variables, 10 samples with the approximate dimensions of a length of 80mm a width of 10mm and a thickness of 2mm, of which the width and thickness have been measured up to 0.01mm accuracy before testing, have been tested on a fixture with a span length of 64mm (see figure 31). The speed of the displacement has been set to 1mm/min. For each sample this results in a measured cross-sectional area and a force/displacement graph. The measurements of width and thickness done on

the 3-point bending samples will also be used for a size analysis.

5.4.a Flexural modulus

The flexural modulus does not give a lot of information about the quality of the productions, since the modulus is mainly dependent on the fiber content which theoretically should be the same for all productions. It does however give an important insight in the potential uses of the produces materials. For most constructions, a high modulus is required for a material to even be considered.

Using equations 6 and 7 the stress/strain curve can be determined. Using the linear part of this graph, between a strain of 0.001 and 0.003, the flexural chord modulus (equation 8) of the sample is determined.

$$\sigma = \frac{3PL}{2bh^2} \quad (6)$$

$$\epsilon = \frac{6\delta h}{L^2} \quad (7)$$

$$E_f^{chord} = \frac{\Delta\sigma}{\Delta\epsilon} \quad (8)$$

Where:

P = being the applied force

L = the support span

b = the width of the sample

h = the thickness of the sample

δ = the midpoint displacement

5.4.b Flexural strength

The flexural strength equals the material stress just before failure and can simply be calculated by inserting the highest force measured before failure into equation 6. The strength of the material helps us to get an indication of the quality of the material. Any imperfections in the material are potential starting points for cracks, which will induce premature failure of the material. In this way differences in the strength between the different tests, can indicate differences in the quality of the process.

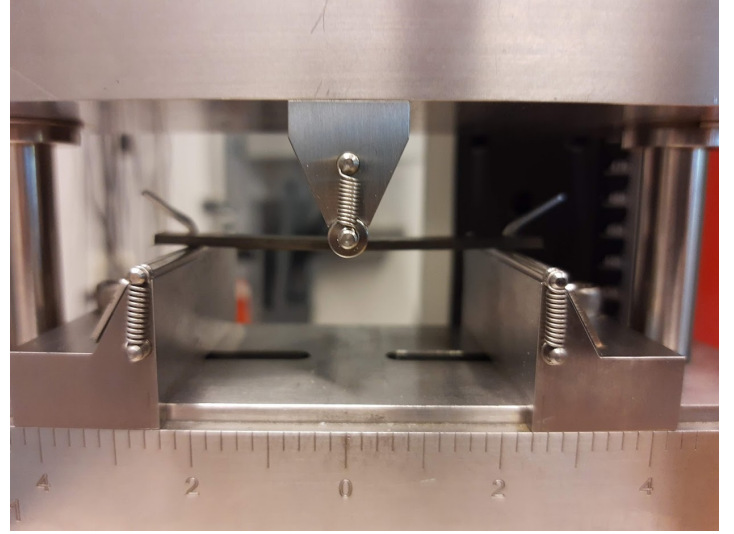


Figure 31: 3-Point bending setup

5.5 Nano-indentation

To get an indication of the polymerization grade of the sample, nano indentation is used. Since the hardness of the polymer is directly related to the polymerization grade, this gives an indication. This technique uses an indenter to probe the material, the maximum force and the depth of indentation can be used together with the shape of the probe to determine the hardness and the indentation modulus. The hardness is determined using equation 9 in which P_{max} is the maximum force used to make the indentation and A_r is the contact area between the indenter and the specimen which is a calibrated function specific to the indenter used. The indentation modulus is determined using the relation seen in equation 10 in which E_{eq} is the indentation modulus, E_{in} and ν_{in} are the indentators modulus and poisson's ratio and ν_{sp} is the poisson's ratio of the specimen. The E^* in this formula is the contact modulus which is determined using equation 11 in which P is the indentation force, R is the radius of the indenter and h is the indentation depth [44].

$$H = \frac{P_{max}}{A_r} \quad (9)$$

$$\frac{1}{E^*} = \frac{(1 - \nu_{in}^2)}{E_{in}} + \frac{(1 - \nu_{sp}^2)}{E_{eq}} \quad (10)$$

$$P = \frac{4}{3} E^* R^{\frac{1}{2}} h^{\frac{3}{2}} \quad (11)$$

Nano-indentation only gives an indication of the local polymerization grade, for this reason a total of 20 indentations are made spread over 2 samples per variable set. From these 20 a significant part will be rejected. For this reason if out of the 20 indentations less than 5 are accepted, more indentations will be done until at least 5 good results are gained.

6 RESULTS AND DISCUSSION

Several pultruded profiles were manufactured using the updated pultrusion line at the University of Twente. An example of the pultruded product is shown in Figure 32. It should be noted that in this thesis only the successful production experiments were analyzed. Some trials did not result in material suitable for testing, or even material at all. Due to time limitations the test with a die entrance temperature of 20°C at 100mm/min pulling speed and the test with a die entrance temperature of 40°C could have not been performed successfully.



Figure 32: Example of a produced sample

Figures 33 and 34 show the sample thickness and width respectively. There are differences present, but these are considered low enough to call it a successful production.

Almost all of the samples were slightly larger than the 2x10mm at which the die cavity was modelled. This was expected due to the gas build-up causing the resin to expand. For the one sample with a smaller thickness it could well be that the vertical force in the roller was too high. This could have caused the sample to be flattened. In this case however an increase in width is also expected. In the case of this sample the width is slightly high, but not higher than the other samples. Alternatively there could have been a higher closing pressure during this test, making the die cavity slightly less high. The one with less wide samples could have been caused by a misalignment in the puller. If the puller pulls towards one side, it is possible that the other side of the die is not properly filled. Also the die plates wear during use, this means that small increase in sample size can be expected over time. The tests with a 20°C die entrance have been performed with new die plates. This means that a small different in the sample size could be caused by inaccuracies during the production of these plates.

The larger variations in the samples with a colder die entrance could be caused by the samples not being fully cured at the die exit. This would allow for small deformations of the samples after leaving the die. This would also explain why it is more present in the 300mm/min samples.

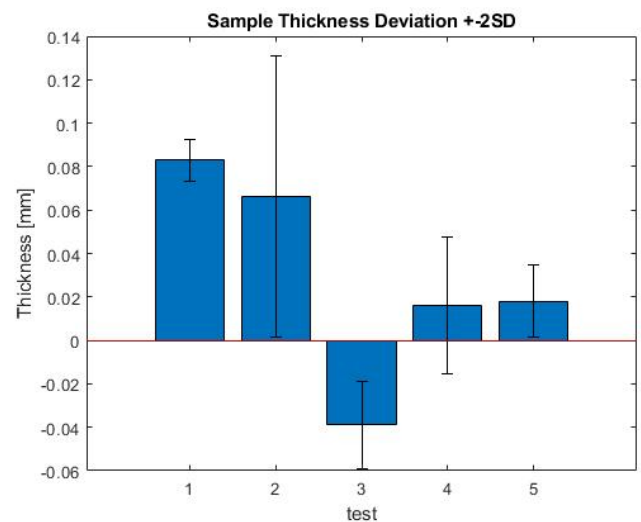


Figure 33: Sample thickness deviation in mm,

- 1: 20-90-110 200mm/min,
- 2: 20-90-110 300mm/min
- 3: 40-90-110 100mm/min,
- 4: 40-90-110 300mm/min
- 5: 40-90-110 300mm/min post cured at 80°C for 1 hour
- 6: 20-90-110 100mm/min glass fibers

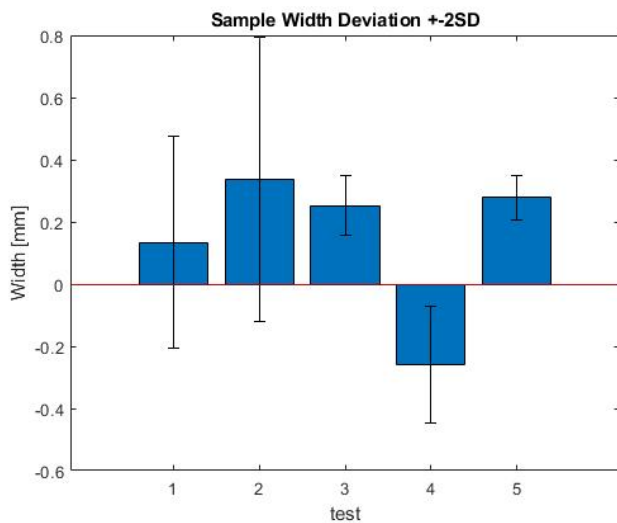


Figure 34: Sample width deviation in mm,
 1: 20-90-110 200mm/min,
 2: 20-90-110 300mm/min
 3: 40-90-110 100mm/min,
 4: 40-90-110 300mm/min
 5: 40-90-110 300mm/min post cured at 80°C for 1 hour
 6: 20-90-110 100mm/min glass fibers

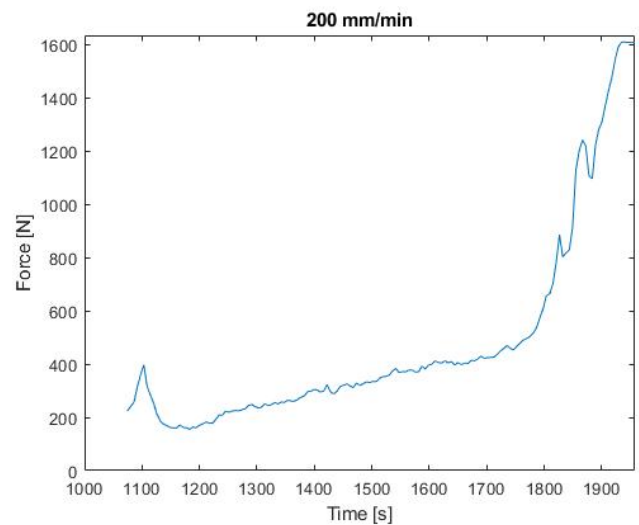


Figure 35: Pulling force over time for the 200mm/min at 20-90-110°C production

in the first 600 seconds are caused by starting the process, for this reason only the material and data is used from after this point in time.

6.1.c 100 mm/min at 40-90-110°C

In the 100mm/min at 40-90-110°C production (see figure 37) the force is smooth with barely any increase for a long period of time. At some point the force quite suddenly increased to higher than the 2000N limit of the force sensor, at which point the production also got stuck. The first 200 seconds of the production are deemed as the startup in this production and therefore the material and data produced in these first 200 seconds are not used for the research. The material used for the tests is from the stable period between 200 and 1100 seconds.

6.1.d 300 mm/min at 40-90-110°C

The 300mm/min at 40-90-110°C production (see figure 38) went less smooth than its 100mm/min equivalent, but still very smooth compared to the large amount of failed productions. After discarding the first 300 seconds of production as startup, the force stayed at a relative stable level for roughly 700 seconds after which an increase started. This increase stayed relatively steady for 400 seconds after which the force jumped up to almost 1600N at which point the production got stuck. The material used for the tests is from the stable period between 300 and 1000 seconds.

6.1 Pulling force

6.1.a 200mm/min at 20-90-110°C

The 200mm/min and 300mm/min at 20-90-110°C productions were done in a single run. Starting at 300mm/min and when a roughly of two meter of product was produced the speed was lowered to 200mm/min. The small peak at the start of the 200mm/min run, as can be seen in figure 35, is caused by the switch in speed. After this a slow and steady increase in the force is seen for most of the run. In the end this increase suddenly becomes significantly steeper, resulting in the process getting stuck. The material used is from the relatively stable period between 1200 and 1800 seconds.

6.1.b 300mm/min at 20-90-110°C

In the 300mm/min (figure 36) production the change in pulling force over time is a lot lower. The graph looks less smooth than the 200mm/min graph, but this is caused by the difference in scale, the 200mm/min has a range of 1600N where in the 300mm/min one it is only 300N. This allows to better observe the small variations in force over time. The large variation

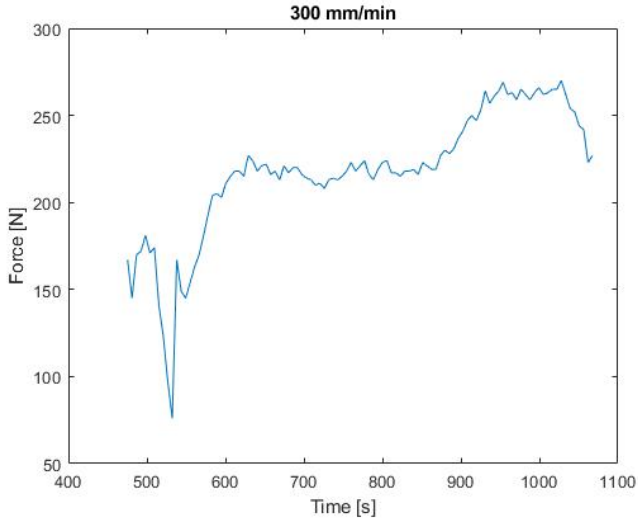


Figure 36: Pulling force over time for the 300mm/min at 20-90-110°C production

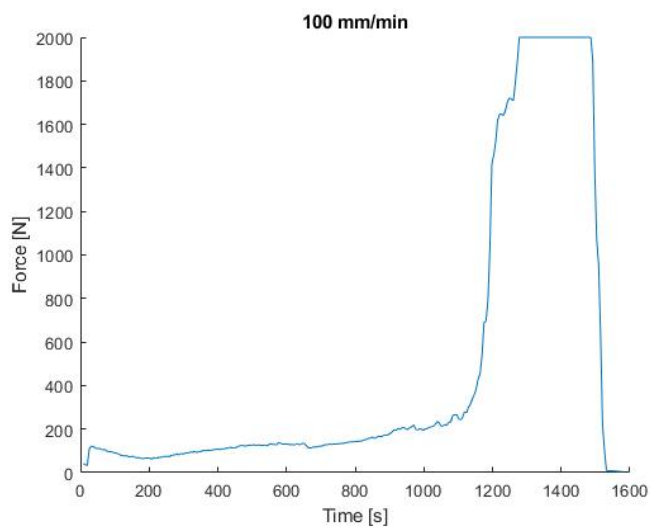


Figure 37: Pulling force over time for the 100mm/min at 40-90-110°C production

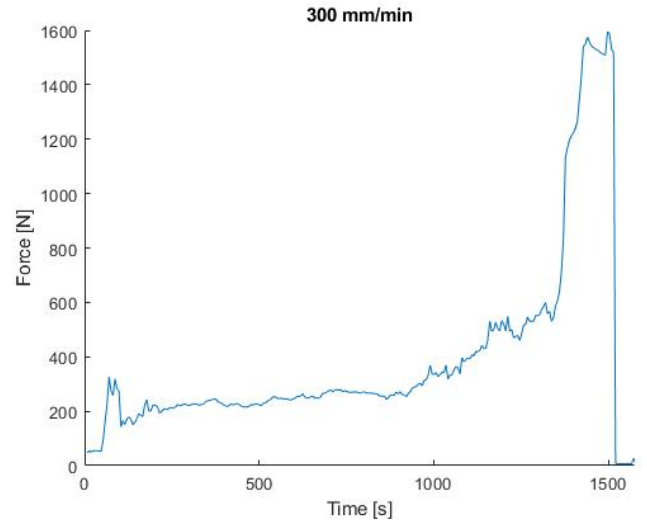


Figure 38: Pulling force over time for the 300mm/min at 40-90-110°C production

Baran et al.[45] has explained that the pulling force can be divided into four parts. The first being the collimation force. This force consists of all frictions which take place before the die. Frictions such as the friction of the bobbin turning on it's holder and the fibers passing over rollers and through guides. This force is very low compared to the others and in general doesn't differ much over time. The second is the bulk force which is caused by the pressure increase at the die entrance. As discussed earlier in section 3.4 this is highly dependant on the viscosity of the material. Since the viscosity is kept low in this research due to the entrance cooler, this force is assumed to remain low. The third is the viscous drag, caused by the liquid resin. It can be approximated by formula 12. In which v_{pull} is the pulling speed, λ is the thickness of the resin layer between the fibers and the die cavity wall, η is the resin viscosity and A is the applicable surface area, from the start of the cavity up to the gel-point. The last is the friction force, caused by the solid material being pressed against the die cavity. It can be approximated using formula 13. In which A is gain the applicable area, but in this case from the gel-point to the detachment point. μ is the friction coefficient and σ the contact pressure.

$$F_{vis} = \frac{v_{pull}}{\lambda} \iint_A \eta(\alpha, T) dA \quad (12)$$

$$F_{fric} = \int_A \mu \sigma dA \quad (13)$$

Even without values for the variables in these two equations, some conclusions can already be made about these forces. For example, the gel-point plays a large role in both of these forces. At the start of the die the viscous drag is present and at the gel-point this switches to the friction force. The location of the gel-point thus determines how much each of these forces play a role. Since the expectation is that the viscous drag is significantly higher than the friction force, it seems beneficial to have a gel-point as close to the entrance as possible. This can be achieved by lowering the pulling speed and/or increasing the die temperature. Taking this in mind a lower pulling forces are expected in the tests at lower speeds, with a higher die entrance temperature. From these productions this is not very clear. The 100mm/min at a 40-90-110°C does have the lowest pulling force which stays well below the 200 N. But the other three tests show no significant differences.

The collimation and bulk forces are in general significantly lower than the viscous and friction forces. In this paper a total for the viscous and friction forces combined is mentioned of roughly 200N for a round die with a similar circumference and pulling speed as the die used in this research, be it for epoxy instead of Elium[®]. Similar values are seen in the stable parts of the carbon Elium[®] tests. Li et al.[46] found values of around 10 times higher, but also with a 10 times higher surface area. Which if compared with the trend found by Baran and taking other differences into account, such as Li using resin infusion, seems reasonable. This indicates that the pulling force during stable production are as expected.

From the four productions, the 300mm/min at 20-90-110°C production is the only one which did not get stuck. Though it needs to be taken into account that the 200mm/min at 20-90-110°C production was done in the same run, by simply lowering the speed. This one showed a steady increase in force from the start. That makes that run the least promising one, as it was just waiting until it had reached a force the puller could not handle. The expectation is that in this case it was the long gel phase, caused by the lower die entrance temperature, which caused

an increase in the friction with the die cavity wall. In the 300mm/min this was possibly not an issue due to methyl methacrylate showing shear thinning behaviour at low shear rates[47], which reduces the friction. Though the gel phase will also have been longer in the 300mm/min production, research into the gell-point and the viscous drag could help understand this.

Both tests with a 40°C die entrance temperature had a relatively steady pulling force until it got stuck. The 100mm/min production even more so than the 300mm/min production. In these two tests it seems the issue is not something that develops over time, but something which happens suddenly. This gives the idea that in these two cases it there where fibers getting stuck, which should result in a relatively sudden stop.

6.2 Microscopy

In this section the micro-structure of the samples will be identified.

6.2.a 200mm/min at 20-90-110°C

These samples (figures 39 and 40) both contained large amounts of voids. In the center there are large voids, most roughly circular and some stretched out. On the sides there are more smaller voids, though some are almost connected in a long line spanning over the entire height of the sample. In the second sample some large resin rich areas are present. The first sample had a fiber volume content of 48% and a void volume content of 7% the second sample had a fiber volume content of 47% and a void content of 6%.

6.2.b 300mm/min at 20-90-110°C

In these samples (figures 41 and 42) a significantly lower amount of voids is seen compared to the 100mm/min equivalent. The same distribution is seen with larger voids in the center of the sample and smaller ones at the sides. In the second sample on the bottom right it looks like some water was still on the sample during the embedding and on the right bottom there seems to be some air trapped between the sample and the epoxy. The first sample had a fiber volume content 52% and a void volume content of 3%, the second sample had a fiber volume content of 52% and void volume content of 3%.

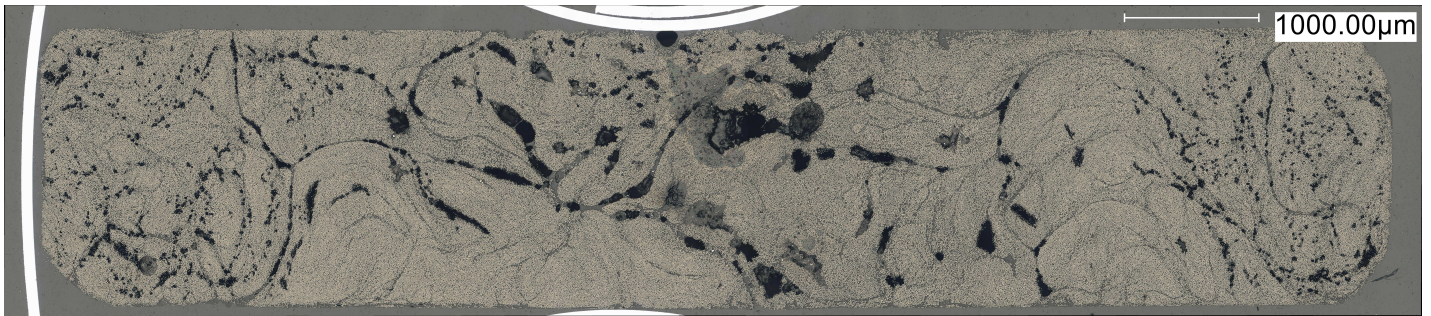


Figure 39: Microscopy of the first sample of the 200mm/min at 20-90-110°C production 700X magnification, fiber volume content 48%, void volume content: 7%

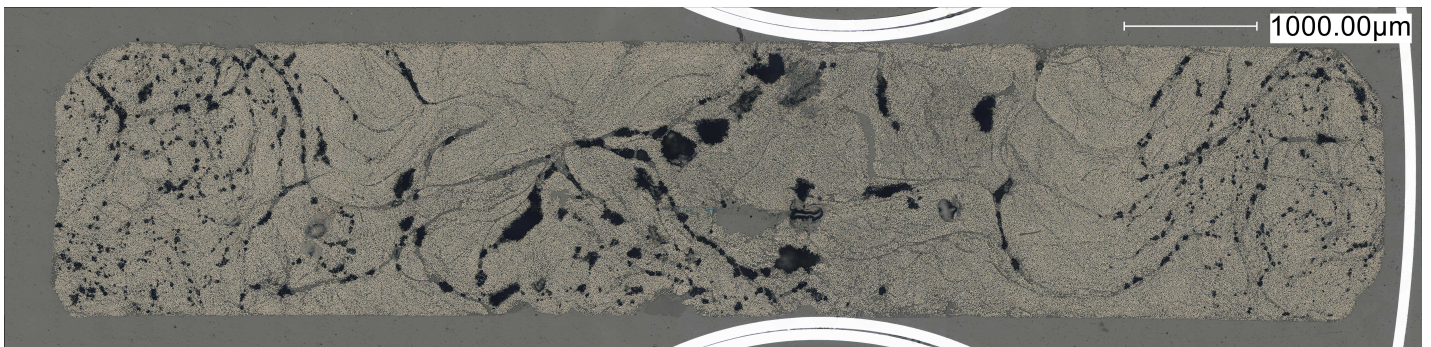


Figure 40: Microscopy of the second sample of the 200mm/min at 20-90-110°C production 700X magnification, fiber volume content: 47%, void volume content: 6%

6.2.c 100mm/min at 40-90-110°C

In these samples (figures 43 and 44) a similar void amount is observed as in the 300mm/min at 20-90-110°C samples. Again the large voids are in the middle and the smaller ones on the sides. Though in these samples the voids are mainly present on one of the sides. Up to a point where the structural integrity of this side was lowered so much that it could be broken of easily. Since the top and bottom side during production is lost during cutting and embedding, the assumption is that though the weak sides are on the opposite sites in these pictures, they were the same side in production. The first sample had a fiber volume content of 50% and a void volume content of 3%, the second sample had a fiber volume content of 52% and a void volume content of 3%.

6.2.d 300mm/min at 40-90-110°C

In these samples (figures 45 and 46) again the same distribution of voids is seen with large voids in the center and small voids on the sides. In sample 1 more and larger voids seem to be present. In sample 2 here is a unidentified obstruction. The initial thought was

that it was simply some filth which ended up on the sample after polishing, but seeing that there seems to be a lack of fibers around this spot indicates that there might be a different issue. For the fiber and void volume analysis this corner has not been taken into account. The first sample had a fiber volume fraction of 49% and a void volume content of 5%, the second sample had a fiber volume content of 50% and a void content of 3%.

6.2.e Volume fractions

The fiber volume fractions (see table 1) are roughly the same for all tests. The value for the 200mm/min at 20-90-110°C test is slightly low and the value for the 300mm/min at 20-90-110°C test is slightly high. The void volume fractions show some more differences with the 100mm/min at 40-90-110°C test having the fewest voids, then the 300mm/min at 20-90-110°C test slightly more, the 300mm/min at 40-90-110°C already has significantly more voids and the 200mm/min at 20-90-110°C test has more than twice as much voids as the 100mm/min at 40-90-110°C test.

From the microscopy images, the 200mm/min at

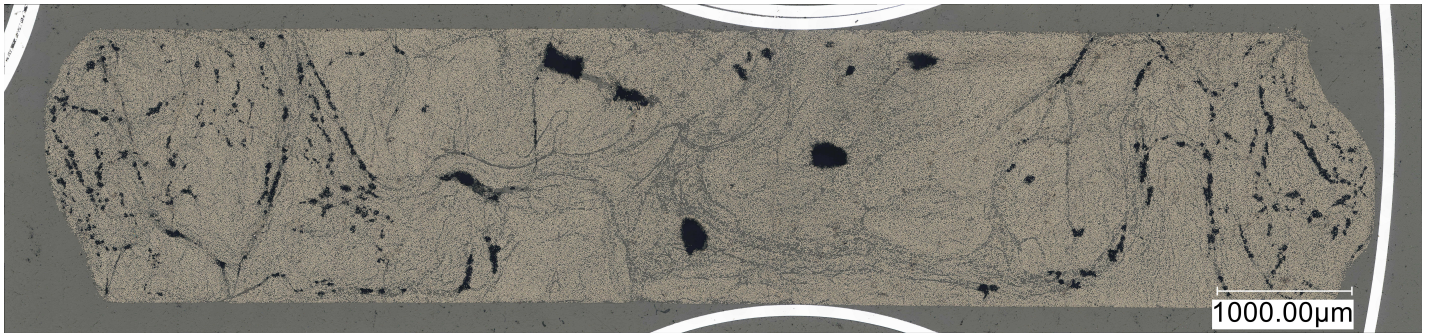


Figure 41: Microscopy of the first sample of the 300mm/min at 20-90-110°C production 700X magnification, fiber volume content: 52%, void volume content: 3%

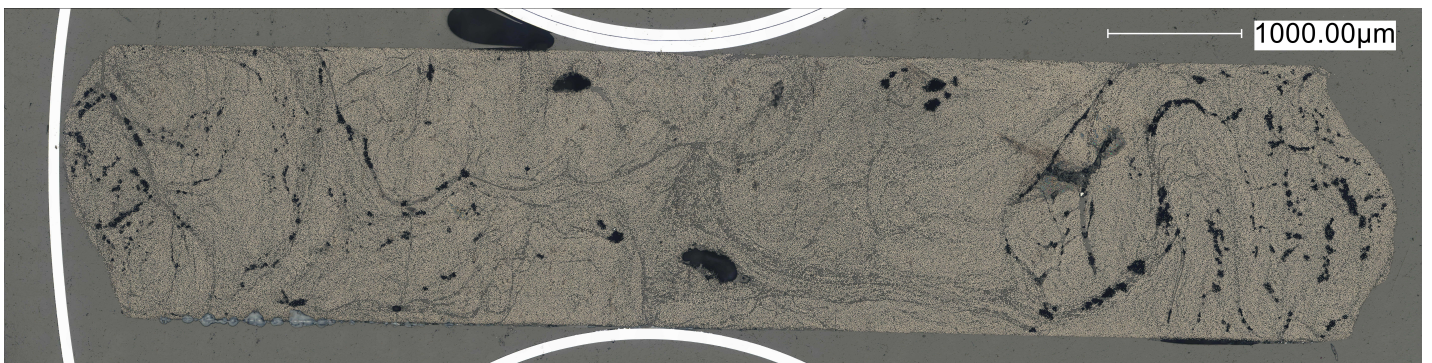


Figure 42: Microscopy of the second sample of the 300mm/min at 20-90-110°C production 700X magnification, fiber volume content: 52%, void volume content: 3%

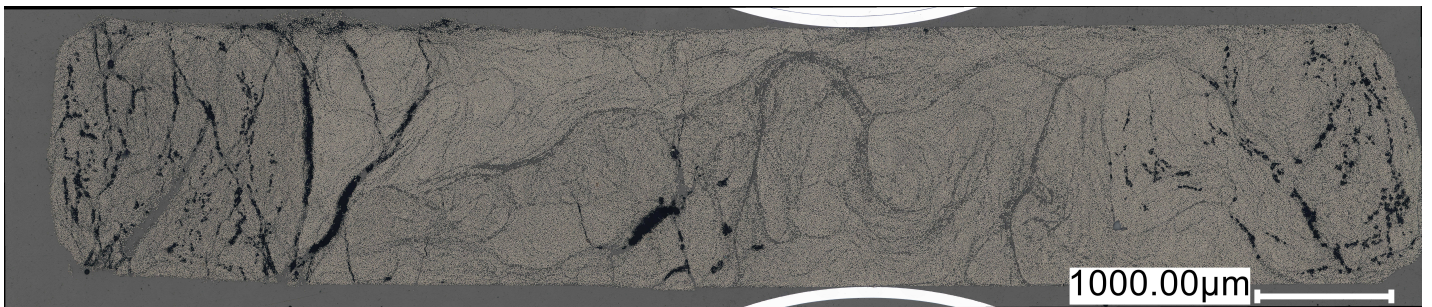


Figure 43: Microscopy of the first sample of the 100mm/min at 40-90-110°C production 700X magnification, fiber volume content: 50%, void volume content: 3%

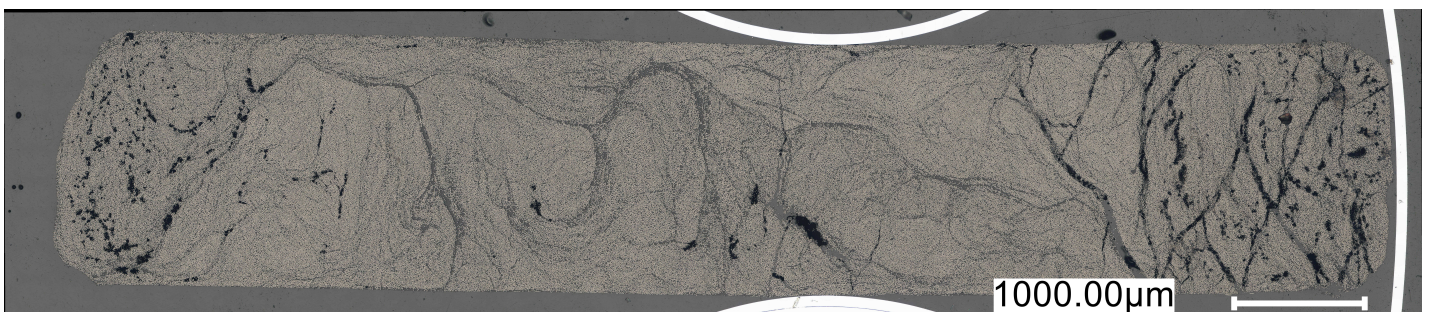


Figure 44: Microscopy of the second sample of the 100mm/min at 40-90-110°C production 700X magnification, fiber volume content: 52%, void volume content: 3%

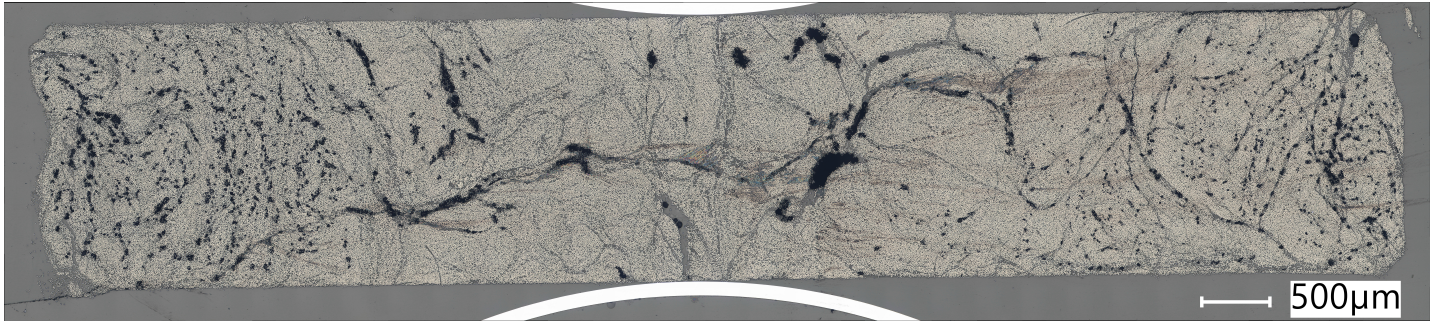


Figure 45: Microscopy of the first sample of the 300mm/min at 40-90-110°C production 700X magnification, fiber volume content: 49%, void volume content: 5%

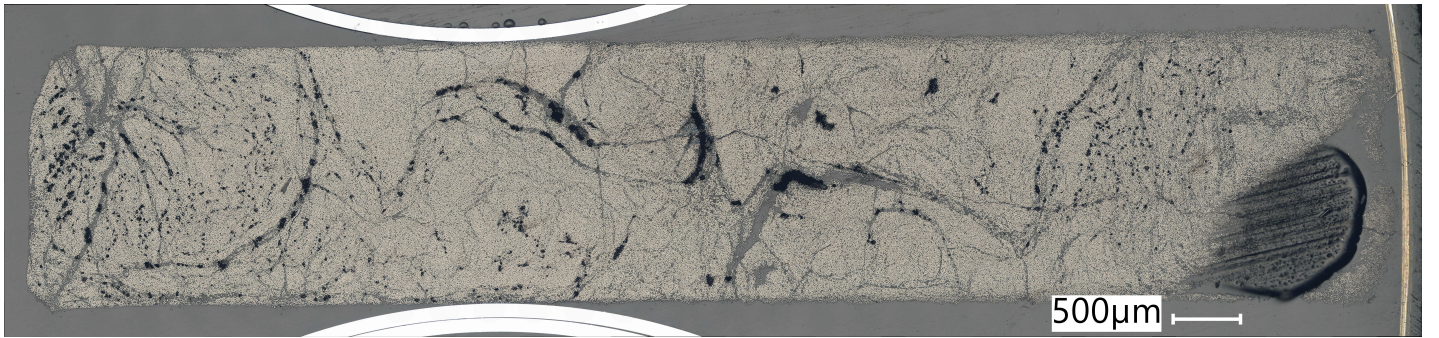


Figure 46: Microscopy of the second sample of the 300mm/min at 40-90-110°C production 700X magnification, fiber volume content: 50%, void volume content: 3%

	20-90-110						40-90-110					
	200			300			100			300		
Sample	1	2	Avg.	1	2	Avg.	1	2	Avg.	1	2	Avg.
Fiber	48,36%	47,10%	47,73%	51,56%	51,70%	51,63%	49,92%	51,51%	50,71%	48,94%	49,91%	49,42%
Void	7,05%	6,08%	6,57%	3,47%	3,00%	3,24%	3,15%	2,70%	2,93%	4,97%	3,10%	4,03%

Table 1: Fiber and void volume contents of the test specimen

20-90-110°C and the 100mm/min at 40-90-110°C seem to be of the worst quality. The 200mm/min at 20-90-110°C has at least 50% more voids than the other samples and the 100mm/min at 40-90-110°C has one side which is so rich in voids it almost falls apart. The 300mm/min at 20-90-110°C seems to be the best form these samples, though when taking the inaccuracy of optical volume measurements into account the difference with the 300mm/min at 40-90-110°C is minimal.

The void content is a debatable subject to take into account for the production quality, since the voids can be caused by aspects besides the process variables. For example the amount of air trapped during the mixing of the resin can have a large influence in the amount of voids. Also the wetting of the fibers could play an important part, which even though the resin bath and guides did not change between the tests, still seemed to vary per production and also over time during productions. The largest voids and Elium[®] rich areas are present in the center of the samples. This may have been caused by the preform orientation which was used, which contained a hole in the middle. This could have caused Elium[®] and air to flow into this hole which would then get stuck in this part of the samples.

The fiber content is roughly the same for all samples, which was expected since, the same bobbins and the same amount of rovings have been used for all tests. The small variation is most likely simply caused by the inaccuracy of the measurement. An interesting observation in the samples is that all of them show resin rich areas which look like flow lines. These lines are especially clear around the center of the sample, and when combined with voids, these lines form a very weak line over the entire thickness of the samples. From all of the productions there were samples which broke in the middle during cutting, most likely due to voids in these lines. These broken samples were not suitable for microscopy and thus not included in this data.

6.3 3 Point bending

In figures 47 till 50 the stress vs strain curves are shown from the 3 point bending tests. Some things are important to notice in these graphs. Both of the

tests at 20-90-110°C show a slower slope at the start which also seems to be exactly the same for each sample. For this reason this part of the graphs is not used in the analysis and the chord modulus has been taken from strains of 0.003 till 0.005 instead of the recommended 0.001 till 0.003. The fact that both of the 20-90-110°C tests show the same slope in combination with the fact that these two tests were done in the same session, gives a strong indication that there was something giving in in the setup itself and not in the sample. Alternatively it could be that these samples were twisted and that this is the part shows the much lower torsion stiffness, though the lack of difference between samples makes this unlikely.

Secondly it is seen that within each test, almost all samples follow the same slope. There is however a single outlier in the 300mm/min at 20-90-110°C test this indicates one sample of a lesser quality. In this test the points of failure also seem more spread out than in the other tests. In the 100mm/min at 40-90-110°C test there are several outliers, which also have some small failures before the full failure. That all samples within a test follow the same slope is a good sign, indicating a stable production with little variations in the sample quality. The one outlier in the 300mm/min at 20-90-110°C test however indicates that this sample was of a lesser quality. In this test the points of failure also seem more spread out than in the other tests, though they seem like clean failures without many small premature failures. The outliers in the 100mm/min at 40-90-110°C test, which also have some small failures before the full failure, indicates that this set of samples had a relatively large amount of imperfections.

The graph in figure 51 shows the flexural chord modulus of the 4 different carbon samples and a glass sample. The red indicates the theoretical value of 137GPa calculated using the rule of mixture for the carbon samples. In the chord moduli only small differences are present between the samples. The 20-90-110°C samples show a slightly lower modulus, with the 300mm/min being a bit lower than the 200mm/min sample. The standard variance for the 20-90-110°C samples is also larger than the standard variance of the 40-90-110°C samples.

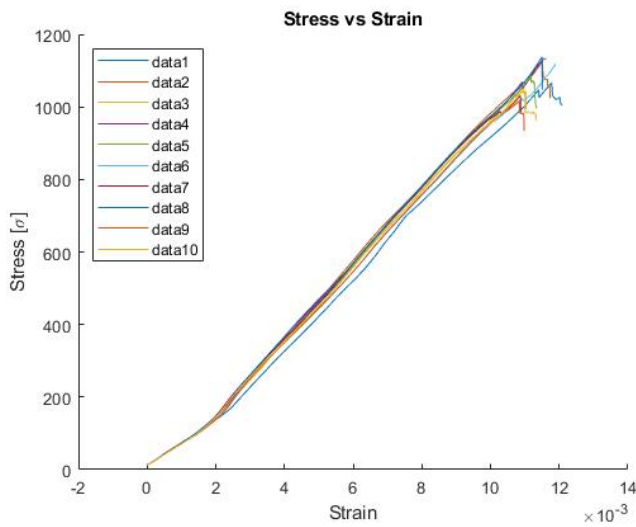


Figure 47: Stress-strain 200mm/min at 20-90-110°C

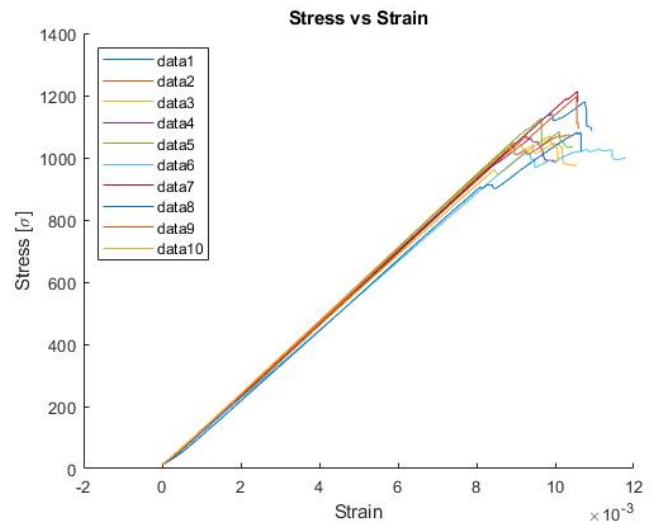


Figure 50: Stress-strain 300mm/min at 40-90-110°C

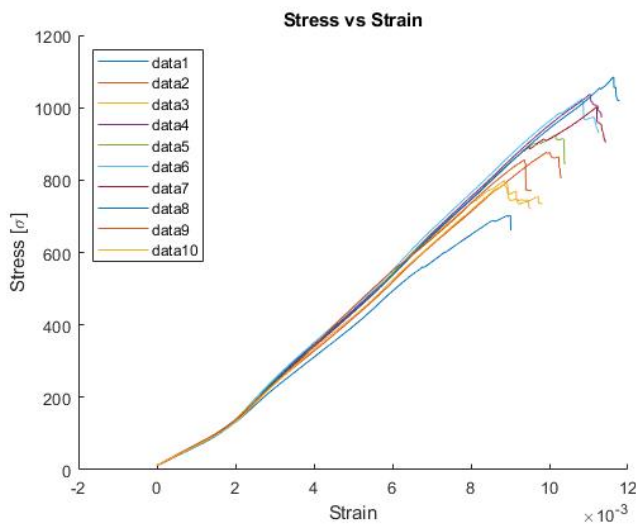


Figure 48: Stress-strain 300mm/min at 20-90-110°C

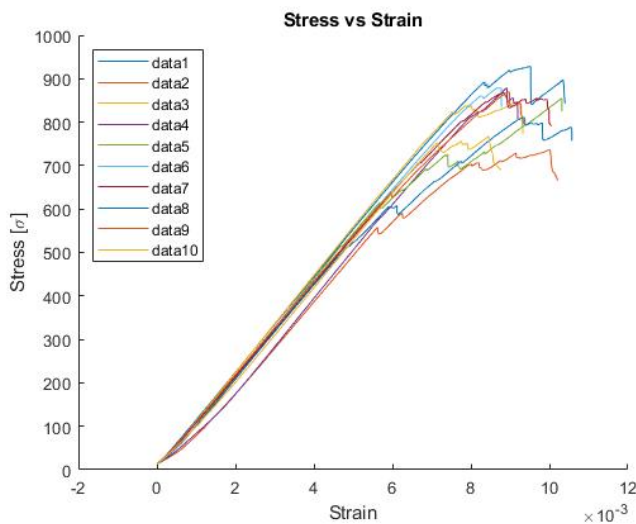


Figure 49: Stress-strain 100mm/min at 40-90-110°C

The graph in figure 52 shows the flexural strength of the the 4 different carbon samples and a glass sample. The theoretical value calculated using the rule of mixture for carbon samples lies at 2.31GPa and has been left out of the figure as to better see the differences between the samples. All values from the tests are significantly lower than the theoretical value.

Similar values are found for the 200mm/min at 20-90-110°C test and the 300mm/min at 40-90-110°C test. The other two carbon samples show significantly lower values.

In the Phd paper of Novo et al.[48], similar research is described on the pultrusion of, among others, carbon polypropylene (PP). The mechanical properties of these carbon PP samples were compared to our samples. The carbon PP samples are deemed good enough for industry use, and can give a nice indication if the same holds for the carbon Elium[®] samples.

On the website of the Röchling Group[8] mechanical properties are mentioned for their spar caps. These values will be used to compare our material to.

On this site 4 different materials are mentioned, being a carbon epoxy, a carbon vinyl ester (VE), a glass vinyl ester and an ultra violet (UV) cured glass epoxy. The flexural properties are not mentioned for the carbon epoxy, therefore the carbon vinyl ester will be used as the comparison (see table 2).

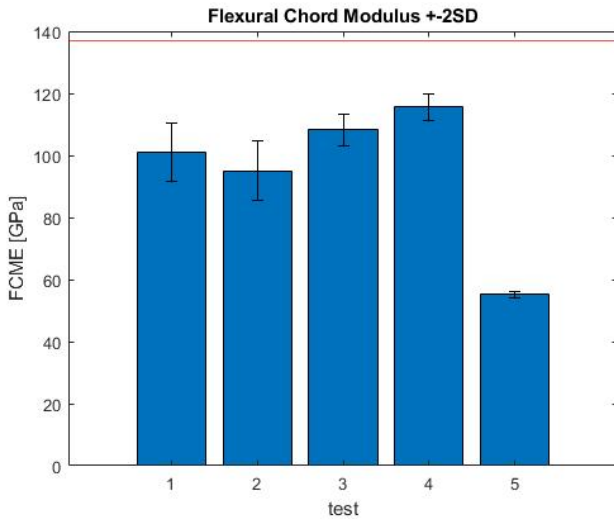


Figure 51: Flexural chord modulus in GPa

$$\epsilon = 3 \cdot 10^{-3} - 5 \cdot 10^{-3},$$

1: 20-90-110 200mm/min

2: 20-90-110 300mm/min

3: 40-90-110 100mm/min

4: 40-90-110 300mm/min

5: 20-90-110 100mm/min glass fibers

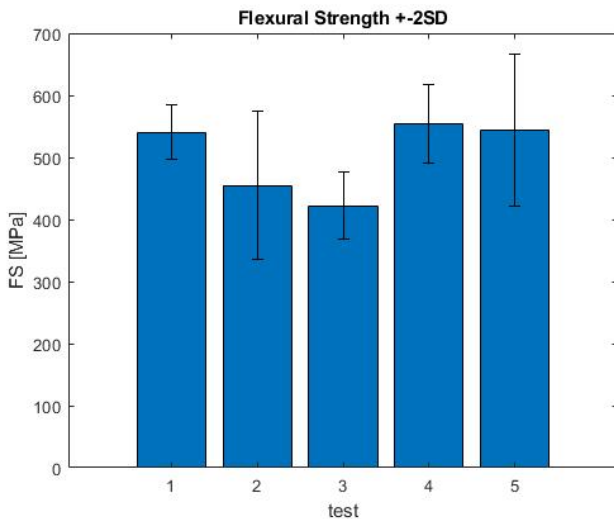


Figure 52: Flexural strength in MPa,

1: 20-90-110 200mm/min

2: 20-90-110 300mm/min

3: 40-90-110 100mm/min

4: 40-90-110 300mm/min

5: 20-90-110 100mm/min glass fibers

The fiber content of the carbon PP samples is about the same as from the carbon Elium[®] samples. The strength of the carbon Elium[®] samples is more than twice as high as that of the carbon PP samples. The flexural modulus is 10GPa higher for the carbon Elium[®] samples. Considering that the carbon PP samples are deemed good enough for use in industry, by extension the same should hold for the carbon Elium[®] samples.

The fiber volume content of this carbon fiber vinyl ester is 65%, which is about 15% higher than was measured in our samples. The flexural strength of the our samples is about half that of the commercial product. This is a big issue since the strength is the usually the limit for carbon fiber spar caps. On this point a lot of improvement is needed to get a material suitable to replace the current ones available. There is potentially a lot of improvement possible, by for example increasing the fiber content and decreasing the void content. The flexural modulus is quite close to the commercial products flexural modulus. This is promising for the potential of carbon Elium[®] becoming a commonly used material.

6.4 Hardness

There are some reasonably big differences in the values (see figure 53) found for the nano-indentation tests for the different sample sets. The 300mm/min at 20-90-110°C and the post cured samples show some of the largest hardness values and the 300mm/min at 40-90-110 together with the glass samples the lowest ones. The standard variance in the tests is very high,

	C-E	C-PP	C-VE
Vf	0.50	0.51	0.65
FS [MPa]	500	240	1200
FS/Vf [MPa]	1000	475	1845
Ef [GPa]	100	90	130
Ef/Vf [GPa]	200	180	200

Table 2: Comparison of the carbon Elium[®] (C-E) to a different research on carbon PP (C-PP)[48] and a commercial product from carbon vinyl ester (C-VE)[8]

even such that all the variances overlap. There is also a large difference in the variance between the different tests.

From the nano-indentation tests, values for the indentation hardness have been found of around 250 MPa. Benaissa et al. [49] has found similar values have been found for PMMA, considering that Elium is a variant of PMMA this seems to indicate that the values found are in the proper range.

The large standard deviation in the indentation hardness measurements means that there are no significant differences between the samples. Most likely the large standard deviation is the caused by several factors including the distance to the closest fiber, contamination of the specimen, sub-surface voids, leftover monomer or peroxide and the local polymerisation.

For the case of nano-indentation of a FRP, the location of the indent can have large effects on the results. Naturally there is the difference between probing in a fiber or in the resin, but from earlier research it has also become clear that the distance to the interface between fiber and resin also affects the results[50]. The fiber behaves softer towards the interface and the resin behaves harder. The change in matrix properties can be the result of several things. Firstly when probing near a fiber there is the possibility that the probe slightly touches the fiber, secondly the matrix close to the fiber is held up by the fiber due to the adhesion between the two and lastly the large heat conductivity of the fibers can result in a increased level of polymerization close to the fiber. The reason for the change of the fiber behaviour is a result of grading. The manufacturing process influences the fiber properties, due to stresses introduced by differences in thermal expansion between the fiber and matrix and as a consequence of the crystallisation[51].

Due to the limited availability of the machines during this research, due to covid-19, the indentation could not always be performed straight after polishing. During the indentations it was noticed that already within 2 hours some contamination's could be seen on the polymer surface. It is unknown whether it is the resin surface reacting due to exposure to air and/or light or dust from the air attaching itself to the surface.

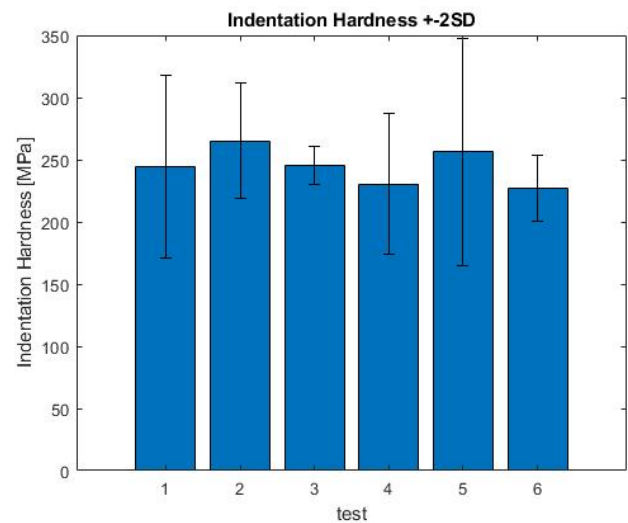


Figure 53: Indentation hardness in MPa,

1: 20-90-110 200mm/min,

2: 20-90-110 300mm/min

3: 40-90-110 100mm/min,

4: 40-90-110 300mm/min

5: 40-90-110 300mm/min post cured at 80°C for 1 hour

6: 20-90-110 100mm/min glass fibers

Sub-surface voids will reduce the hardness measured, by allowing the polymer to be pushed into the void instead of being pressed against the underlying polymer. Voids very close to the surface might be seen with the microscopy due to the Elium® opacity being low, but deeper voids can not be seen and might still influence the results.

The resin consists of a monomer, a peroxide and a release agent. The mixing of these components is never perfect. Therefore there will be regions in the end product which contain some leftover peroxide and/or more release agent. These "contamination's" can influence the hardness measured at these points. The leftover peroxide is in a powder form, this will behave harder, as it will not push back when the indenter is removed. The release agent will locally make the resin behave softer, by making it more liquid and sticky in its behaviour.

7 CONCLUSION

The goal of this research was to gain fundamental knowledge on the pultrusion of carbon fiber with Elium[®] resin by the pultrusion process. On this subject a significant improvement has been made throughout the research. In the beginning of the research a pultrusion with carbon fibers and Elium[®] had never been performed. The question was thus even whether it would work at all. Towards the end of the research UD carbon Elium[®] has successfully been created with satisfactory mechanical properties.

A model has been made to help understand the resin flows at the die entrance, which can be used to increase the understanding further. And indicates the importance of the viscosity at the die entrance.

It has been observed that the addition of an entrance cooler works beneficial to the pultrusion of carbon fiber with Elium[®]. Keeping the die entrance below the initiation temperature of 50°C has proven to reduce to the pile-up of solidified resin at the die entrance to almost zero. Specifically in the setup used in this research a winch has proven useful for the start-up of the process. The physical needs of the operator have been lowered and the safety of the operator is increased. Some other aspects came up during the research which will need improvements, but which have not yet been improved during this research. These things include the 4-part die which could be improved by switching to a 2-part die. As to reduce the risk of leakages and fibers getting stuck. The puller, which could be improved by switching to an area-load instead of a line-load, with a caterpillar puller for example. This could reduce the damage done to the material at the puller. Either an expensive chrome coating is needed for the die cavity, or a research into the friction of the cavity wall with the resin and the degradation of cavity wall is needed. This to improve the reliability of the process by preventing friction forces in the die to become too high.

The first objective was to investigate the evolution of the pulling force during the pultrusion process. During the research it has become clear that the pulling force can well be used to monitor the pultrusion process. The force gives off a warning before the process starts to fail by showing an increase in

force. Two different reasons for the pultrusion getting stuck have been observed during this research each resulting in a different signature in the pulling force. The first being, the resin having too much friction with the die, this resulted in a steadily increasing force over a longer time. Eventually this force would become too high, resulting in the process getting stuck. If noticed on time, this failure could be postponed by increasing the pulling speed, but for a steady continuous production that is of course unwanted.

The second objective was to determine the flexural modulus and strength of the pultruded carbon Elium[®] composites. A flexural modulus was found of around 100GPa and a flexural strength was found of around 500MPa. The flexural stiffness of the successful productions is close to that of commercially available spar caps and similar to previous research on carbon fiber thermoplastic pultrusion. The flexural strength however is very low and needs significant improvement before it can compete with the current market. The currently produced material has a relatively low fiber volume content of roughly 50% and contains a lot of voids. This means that by increasing the fiber volume content and by finding ways of decreasing the amount of voids, degassing for example, a significant improvement is possible.

The third objective was to describe the final degree of curing by means of hardness measurements. The hardness values measured, are close to what can be expected from cured Elium[®], indicating a fully cured sample. The variance in the data however is very big, which indicates that either the level of cure varies over the sample, or that nano-indentation is not a suitable technique for local cure determinations. Most likely it is combination of both. On the samples differences in colour were seen, which could indicate less cured areas and it is known that the presence of a fiber and the distance to said fiber influence the hardness measured.

The last objective was to correlate pulling speed and die entrance temperature with the resulting microstructure, hardness and mechanical performance. The die entrance temperature proved to have a large impact on the process and the produced material. As already mentioned, the die entrance temperature needs to be lower than the initiation temperature of the resin of 50°C to prevent solid resin to clog the

die entrance. For this reason two temperatures below 50°C have been tested being 20°C and 40°C. During production it was seen that the material leaving the die in the case of the 20°C die entrance was not fully cured, whereas in the 40°C it was fully cured. There was no significant difference in the resin build-up at the die entrance. Thus with the higher temperature resulting in potentially faster productions a temperature close to the initiation temperature can be recommended. Though since the highest tested in this research was 40°C, there is still some doubt about whether there will be issues when getting too close to the initiation temperature.

Similar as to how a lower temperature results in a lower level of cure, a higher speed also results in a lower level of cure. This was also seen during this research where the 300mm/min production with a 20°C die entrance become stiff sooner than the 200mm/min production. Though a high production speed is wanted, so a balance is needed between the temperatures and the pulling speed. During this research it was found that with a 20°C die entrance at 200mm/min and at 300mm/min the material was not fully cured, but an increase of cure was seen with the 200mm/min compared to the 300mm/min. Also in both cases the material cured enough between the die exit and the roller to become stiff enough for the roller to pull it properly. This indicates that it is possible to use a 20°C die entrance if the speed is lower. With the die entrance at 40°C, both the 100mm/min and the 300mm/min productions were already stiff at the die exit.

The lower speeds resulted in the worst microstructures, with the 100mm/min samples having a side which fell apart with much ease and the 200mm/min samples containing both many and large voids. The temperature does not seem to have a large influence, but the void content in the samples at 300mm/min at 20°C does have a lower void content than the samples at the same speed at 40°C.

The variances of the hardness of all the samples overlap, meaning that a proper conclusion cannot be made.

The flexural modulus for the different speeds and die entrance temperatures are similar. The 40°C samples have a slightly higher modulus compared to

the 20°C samples. This could be caused by a higher degree of cure, assuming that the hardness tests are not a proper measurement for this. The differences between the different speeds are not significant. In the flexural strength some large differences are found, but they don't seem to correlate to either the speed or temperature. Most likely the imperfections which influence the strength are a result of multiple variables in both the production procedure and the test setup.

From the currently tested variables the 300mm/min at 40-90-110°C set seems the most promising. By increasing the entrance temperature closer to 50°C, potentially higher speeds could be used. This however is highly setup dependent, meaning that care always needs to be taken and that adjustments to pulling speed and/or die entrance temperatures must be made according to observations made.

8 RECOMMENDATIONS

In this section some recommendations will be made for the setup at the UT and for the future of this specific project in particular. Some of these recommendations have already been mentioned earlier in this report, but will be mentioned again to get a nice gathered summary.

During this research only 4 different combinations of variables have been tested. A significantly higher number is needed to find an optimum. Preferably every test should also be performed several times, to reduce the influence of the operator and environmental aspects on the results. Since the results of this are very dependant on the setup, it is recommended to suspend these tests, until no more changes to the setup are expected.

The preform orientation used contained a hole in the center. This could have been the reason for the high amounts of voids and resin in the center of the samples. For this reason a different orientation is recommended. For example the orientation as shown in figure 54. This is however not tested yet, and will thus require experimental validation.

During this research a puller was used consisting out of 2 steel rolls. This resulted in a line pressure to be applied to the finished product. During productions with relatively high pulling forces, this meant also a higher line pressure, some damages were seen on the product due to this pressure. Such as flattened out samples and broken fibers on the sample surface.

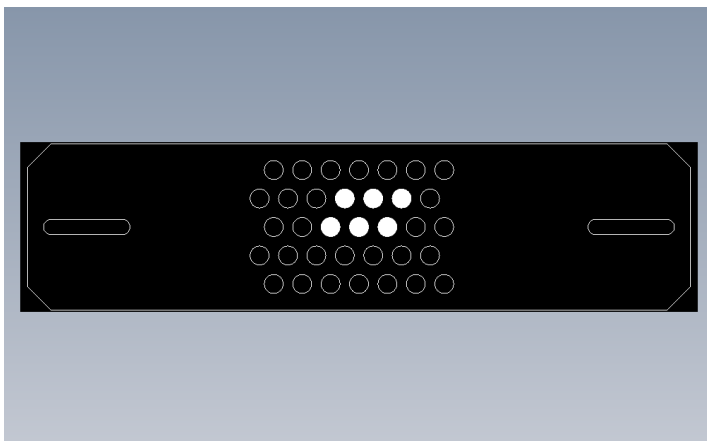


Figure 54: Recommended fiber preform orientation. The holes which should be used are shown in white.

Therefore it is recommended to switch to a puller which applies an area pressure instead. For example a caterpillar puller could be used. This was also mentioned by the designer of this setup Jasper van Meurs in his thesis "Building a laboratory-scale pultrusion line"[52].

As also already mentioned by Jasper van Meurs[52], the die plates currently in use are not up to the industry standards. Currently simple laser-cut stainless steel plates are used, which are only polished by hand. Resulting in plates which cause a relatively high amount of friction and which degrade fast when used. Normally chrome coated dies are used, but the cost of those are many times higher than the ones currently used. This means that there is a choice to be made between more reliable productions and easy and cheap replacements. For this specific research focused setup the stainless steel plates without coating are recommended, but a research into the degradation of these plates and the influence on the pulling force/friction could be useful. Hopefully leading into a guide on how to clean and polish the plates and a rough estimation on when a plate needs replacing.

Some issues do remain in the setup. The process always seems to get stuck after some time (as was also mentioned by the designer[52]), despite the addition of the die entrance cooler. Some signs of potential reasons were seen during the tests. The two main reasons seen are resin leakages between the die plates and fibers getting stuck between the die plates. The pressure in the die causes resin to flow between the die plates if they don't close properly. These resin leakages solidify over time, creating an obstacle for the resin behind it. This resin then also gets stuck, in this way creating an obstacle which grows over time. The moving material can break small obstacles loose, but when an obstacle becomes too big, the pulling force increases steadily until the whole production comes to a halt. An example of resin leaking from the mould can be seen in figure 56 and the result on the end product, when removed from the die after it got stuck, in figure 55.

With the resin flow into the interfaces, sometimes also some fibers flow into the interfaces. If these fibers get stuck there, the part of the fiber behind it will keep moving. This causes the fiber to fold, thereby



Figure 55: Resulting product when opening the die after it got stuck due to resin leakages

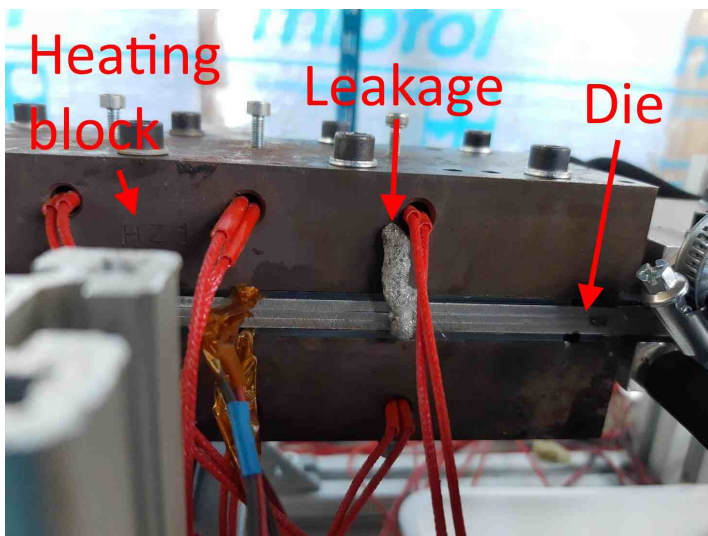


Figure 56: Resin leaking out of the mold

increasing the room it needs. This then results in more fibers being pushed into the interface and also getting stuck. Sometimes the fiber breaks and the process can continue with only a small weak point being created in the final material. But if the fiber does not break, the pulling force increases rapidly until the process comes to a halt. Figure 57 some broken fibers are seen which were found in between the die plates after opening them up. In figure 58 an image is seen of when the fibers don't break. The expectation of what occurred is the following. In the middle right of the image some fibers got stuck. The rest of the material kept moving, but behind this the fibers couldn't move past the first blockade, creating a high pressure zone which caused the big bulge of material to get stuck in between the plates. This caused the process to come to a halt, but due to the pullers still pulling, very high forces were put on the material between the blockade and the puller, causing lengthwise cracks.

Both these issues are related to the die plates not closing properly, indicating that there is much to win if a way is found to improve the closing of the die. The first step in this has already been performed, but has not been properly tested during this research. The worn out M5 bolts with thread in the heating blocks have been replaced with M8 bolts all the way through with nuts on top instead of the thread in the blocks. This increases the maximum clamping force and allows for the nuts and bolts to be easily replaced when worn out. The new bolts have not yet been properly tested, and a conclusion about how well they work can not yet be made.

A different option for improvement is to reduce the amount of places where leakages can take place. The current die consists out of 4 die plates, resulting in 4 interfaces where resin can leak and fibers can get stuck. This amount can already be halved by switching to a 2 part die. By switching to a two-part die, a top and bottom with the cavity milled out, the amount of interfaces is halved which hopefully reduces the amount of leakages and fibers getting stuck. This will however reduce the ease and increase the cost of replacing the die significantly, so more thought about the materials, coatings and treatments could be beneficial. A 1 part die would remove all the interfaces, but this is almost impossible to produce and to clean after use.

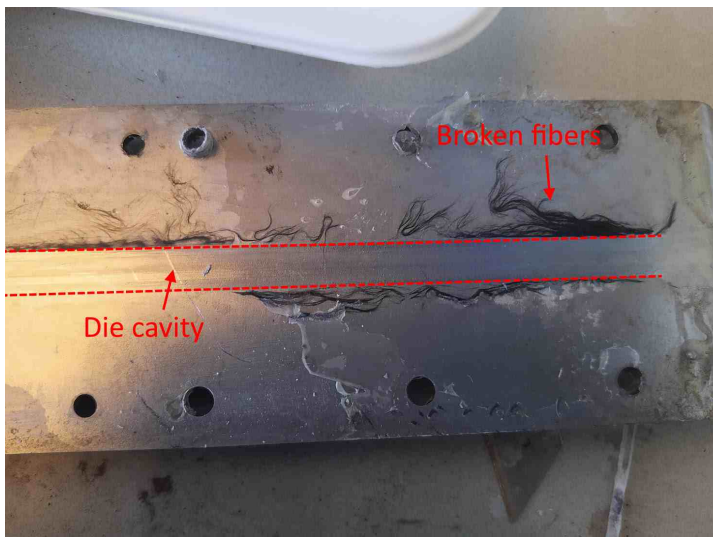


Figure 57: Broken fibers found between plates after production

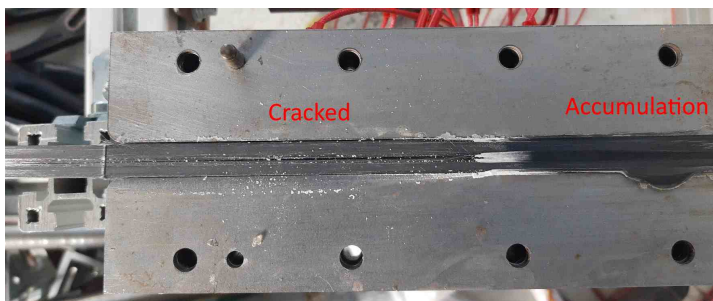


Figure 58: Inside of die cavity after fibers got stuck

The temperatures of the heating zones have been kept constant during this research, but higher temperatures could be beneficial to the process. Especially when the entrance is cooled to below 50°C, removing the risk of solidification at the entrance, higher temperatures should not cause too many issues. A thing that does need to be taken into account is the boiling temperature of Elium® of 100°C. This temperature should not be reached before the resin is in the gel phase, otherwise even more gas will be present in the material. A rheology test at 90°C could help to get an estimation for the gel-point in the die.

It would be beneficial for the process to have a as short as possible gel-phase. The gel state is expected to cause the most friction. Also any leakages in the gel-phase area of the die will solidify over time, this could cause blockages in the die. Fibers getting caught between the die interfaces are a risk in both the liquid and gel-phase. Therefore preferentially both should be kept as low as possible, but with the lower limit that the polymerisation is not allowed to start before the die entrance and that boiling should not occur. Which in practice comes to a die entrance temperature of below 50°C (the required length of this section depends on the pulling speed) and after that a section of below 100°C.

It would be interesting to find out the friction differences for different stages of the polymerisation. For example a test could be done at a die temperature of below 50°C, in this scenario the Elium® will not polymerise. The pulling force can then be divided by the die cavity surface area to find the frictions force per area. The same can be done with the die at different temperatures. If combined with DSC tests, it can be estimated how far in the die the material will be in a specific part of its polymerisation. For the solid state a finished product can be used and pulled over a piece of the same material as the die with a known force being applied from the top and the pulling force being measured, to also find this friction coefficient.

Several improvements can be made to the model to make it more useful. Firstly a investigation of the viscosity change during polymerisation could implement that change in the model. The heat profile of the reaction can already be obtained from a DSC

test allowing to model the polymerisation speed. The before mentioned friction estimations can be used to implement a formula for the shear force applied on the walls of the die cavity instead of the currently used no-slip condition. With these implemented, and if the model is extended to the full 400mm the pulling force can be properly estimated from the model.

The permeability of the fibers in the model is currently isotropic. An implementation in which a differentiation is made between the permeability in fiber direction and orthogonal to it would be beneficial to the accuracy of the model.

To improve the computational speed of the model a symmetry can be applied. This has not been done yet, since the speed was considered acceptable and this full model gives a nicer view. Currently gravity is implemented, which limits the option for a second symmetry, but if the gravity implementation is considered redundant, another symmetry plane can be implemented to further improve the processing time.

REFERENCES

1. Wind Europe, Wind in power 2017, annual combined on-shore and offshore wind energy statistics, *Published February*, (2018).
2. Anders Arvesen and Edgar G Hertwich, Assessing the life cycle environmental impacts of wind power: A review of present knowledge and research needs, *Renewable and sustainable energy reviews*, (2012), 16(8):5994–6006.
3. Per Dannemand Andersen, Mads Borup, and Thomas Krogh, Managing long-term environmental aspects of wind turbines: a prospective case study, *International Journal of Technology, Policy and Management*, (2007), 7(4):339–354.
4. Valentin Sommer, Jan Stockscläder, and Grit Walther, Estimation of glass and carbon fiber reinforced plastic waste from end-of-life rotor blades of wind power plants within the european union, *Waste Management*, (2020), 115:83–94.
5. F. Arias, Assessment of present/future decommissioned wind blade fiber-reinforced composite material in the united states, *Independent Study, Dept. of Civil Engineering, City College of New York, United States*, (2016).
6. Anaële Lefeuvre, Sébastien Garnier, Leslie Jacquemin, Baptiste Pillain, and Guido Sonnemann, Anticipating in-use stocks of carbon fibre reinforced polymers and related waste generated by the wind power sector until 2050, *Resources, Conservation and Recycling*, (2019), 141:30–39.
7. Robynne Murray, David R Snowberg, Derek S Berry, Ryan Beach, Samantha A Rooney, and Dana Swan, Manufacturing a 9-meter thermoplastic composite wind turbine blade, Technical report, National Renewable Energy Lab.(NREL), Golden, CO (United States), (2017).
8. <https://www.roechling.com/industrial/renewable-energies/wind-energy/materials-for-wind-turbine-blades/spar-caps-for-wind-turbines>, urldate = 2021-08-06.
9. Shanmugam L. Lu D. Wang X. Wang B. Yang J. Kazemi, M. E., Mechanical properties and failure modes of hybrid fiber reinforced polymer composites with a novel liquid thermoplastic resin, elium®, *Composites Part A: Applied Science and Manufacturing*, (2019), 125:105523.
10. Somen K Bhudolia, Pavel Perrotey, and Sunil C Joshi, Mode I fracture toughness and fractographic investigation of carbon fibre composites with liquid methylmethacrylate thermoplastic matrix, *Composites Part B: Engineering*, (2018), 134:246–253.
11. Somen K Bhudolia, Sunil C Joshi, Anthony Bert, Boon Yi Di, Raama Makam, and Goram Gohel, Flexural characteristics of novel carbon methylmethacrylate composites, *Composites Communications*, (2019), 13:129–133.
12. Escalé P. Gerard P. Zoller, A., Pultrusion of bendable continuous fibers reinforced composites with reactive acrylic thermoplastic elium® resin, *Frontiers in Materials*, (2019), 6:290.
13. Olivia de Andrade Raponi, Lorena Cristina Miranda Barbosa, Bárbara Righetti de Souza, and Antonio Carlos Ancelotti Junior, Study of the influence of initiator content in the polymerization reaction of a thermoplastic liquid resin for advanced composite manufacturing, *Advances in Polymer Technology*, (2018), 37(8):3579–3587.
14. Chen-Chi M Ma and Chin-Hsing Chen, Pultruded fiber-reinforced poly (methyl methacrylate) composites. i. effect of processing parameters on mechanical properties, *Journal of applied polymer science*, (1992), 44(5):807–817.
15. R El-Hajjar, H Tan, and KM Pillai, Advanced processing techniques for composite materials for structural applications, In: , *Developments in Fiber-Reinforced Polymer (FRP) Composites for Civil Engineering*. Elsevier, (2013), 54–77e.
16. AM Fairuz, SM Sapuan, ES Zainudin, and CNA Jaafar, Polymer composite manufacturing using a pultrusion process: a review, *American Journal of Applied Sciences*, (2014), 11(10):1798.
17. Ismet Baran, Pultrusion processes for composite manufacture, In: , *Advances in Composites Manufacturing and Process Design*. Elsevier, (2015), 379–414.
18. Dodds N. Hale J. M. Gibson A. G. Miller, A. H., High speed pultrusion of thermoplastic matrix composites, *Composites Part A: Applied Science and Manufacturing*, (1998), 29(7):773–782.
19. Muhammad S Irfan, Nicholas Shotton-Gale, Mark A Paget, Venkata R Machavaram, Colin Leek, Shane Wootton, Mark Hudson, Stefan Helmsmans, Francisco N Bogonez, Surya D Pandita, et al., A modified pultrusion process, *Journal of Composite Materials*, (2017), 51(13):1925–1941.
20. Sana Koubaa, Steven Le Corre, and Christian Burtin, Thermoplastic pultrusion process: Modeling and optimal conditions for fibers impregnation, *Journal of Reinforced Plastics and Composites*, (2013), 32(17):1285–1294.
21. Ke Chen, Mingyin Jia, Hua Sun, and Ping Xue, Thermoplastic reaction injection pultrusion for continuous glass fiber-reinforced polyamide-6 composites, *Materials*, (2019), 12(3):463.
22. Dutta K. Ray B. C. Mahato, K. K., Static and dynamic behavior of fibrous polymeric composite materials at different environmental conditions, *Journal of Polymers and the Environment*, (2018), 26(3):1024–1050.

23. Akkerman R. Warnet L., *Composites Course 2017-2018*, – University of Twente, (2017).
24. U.O. Wisconson, Diamond, and graphite, <http://www.chem.wisc.edu/~newtrad/CurrRef/BDGTopic/>, (2012), Accessed on 2020-04-07.
25. Hayakawa E. Shioya, M. and A. Takaku, Non-hookean stress-strain response and changes in crystallite orientation of carbon fibers, *Journal of Material Science*, (1996), 31.
26. H. Derek, *An introduction to composite materials*, Cambridge university press, (1981).
27. Peijs T. Van den Oever, M., Continuous-glass-fibre-reinforced polypropylene composites ii. influence of maleic-anhydride modified polypropylene on fatigue behaviour, *Composites Part A: Applied Science and Manufacturing*, (1998), 29(3):227–239.
28. Alexander Vedernikov, Alexander Safonov, Fausto Tucci, Pierpaolo Carlone, and Iskander Akhatov, Pultruded materials and structures: A review, *Journal of Composite Materials*, (2020), 0021998320922894.
29. A. R. Offringa, Thermoplastic composites—rapid processing applications, *Composites Part A: Applied Science and Manufacturing*, (1996), 27(4):329–336.
30. Peperkamp M.W. Boiten D.A., Forming behaviour of sandwich composites, (2019).
31. Cong W. Qiu J. Wei J. Wang S. Ning, F., Additive manufacturing of carbon fiber reinforced thermoplastic composites using fused deposition modeling, *Composites Part B: Engineering*, (2015), 80:369–378.
32. Congze Fan, Zhongde Shan, Guisheng Zou, Li Zhan, and Dongdong Yan, Interfacial bonding mechanism and mechanical performance of continuous fiber reinforced composites in additive manufacturing, *Chinese Journal of Mechanical Engineering*, (2021), 34(1):1–11.
33. Ulrich Sachs, *Friction and bending in thermoplastic composites forming processes*, University of Twente, (2014).
34. Hojjati M. Immarigeon J. P. Yousefpour, A., Fusion bonding/welding of thermoplastic composites, *Journal of Thermoplastic composite materials*, (2004), 17(4):303–341.
35. Goram Gohel, Somen K Bhudolia, Jayaram Kantipudi, Leong Kah Fai, and Robert J Barsotti Jr, Ultrasonic welding of novel carbon/elium® with carbon/epoxy composites, *Composites Communications*, (2020), 100463.
36. Life Soul Magazine’s Chief Rosa Medea, Wikado playground: Kids playground built from discarded wind turbine parts, (2017).
37. Dylan S Cousins, Yasuhito Suzuki, Robynne E Murray, Joseph R Samaniuk, and Aaron P Stebner, Recycling glass fiber thermoplastic composites from wind turbine blades, *Journal of cleaner production*, (2019), 209:1252–1263.
38. Lawrence C Bank, Franco R Arias, Ardavan Yazdanbakhsh, T Russell Gentry, Tristan Al-Haddad, Jian-Fei Chen, and Ruth Morrow, Concepts for reusing composite materials from decommissioned wind turbine blades in affordable housing, *Recycling*, (2018), 3(1):3.
39. Life Soul Magazine’s Chief Rosa Medea, Wikado playground: Kids playground built from discarded wind turbine parts, (2021).
40. D Sharma, TA McCarty, JA Roux, and JG Vaughan, Fluid mechanics analysis of a two-dimensional pultrusion die inlet, *Polymer Engineering & Science*, (1998), 38(10):1611–1622.
41. KS Raper, JA Roux, TA McCarty, and JG Vaughan, Investigation of the pressure behavior in a pultrusion die for graphite/epoxy composites, *Composites Part A: applied science and manufacturing*, (1999), 30(9):1123–1132.
42. Composite Materials Handbook-17 (CMH-17), SAE International on behalf of CMH-17, a division of Wichita State University, (2012).
43. ASTM International, *Standard test method for flexural properties of polymer matrix composite materials*, ASTM International, (2015).
44. VI Kushch, SN Dub, and PM Litvin, Determination of the young modulus from elastic section of the berkovich indenter loading curve, *Journal of Superhard Materials*, (2007), 29(4):228–234.
45. Ismet Baran, Pierpaolo Carlone, Jesper Hattel, Gaetano S Palazzo, and Remko Akkerman, The effect of product size on the pulling force in pultrusion, In: *Proc. , Key engineering materials*, volume 611. Trans Tech Publ, (2014), 1763–1770.
46. Shoujie Li, Liqun Xu, Zhongman Ding, L James Lee, and Herbert Engelen, Experimental and theoretical analysis of pulling force in pultrusion and resin injection pultrusion (rip)—part i: experimental, *Journal of composite materials*, (2003), 37(2):163–189.
47. Ian Wagstaff and Charles E Chaffey, Shear thinning and thickening rheology: I. concentrated acrylic dispersions, *Journal of Colloid and Interface Science*, (1977), 59(1):53–62.
48. PJ Novo, JF Silva, JP Nunes, and AT Marques, Optimizing the production and processing of fibre reinforced thermoplastic pre-impregnated materials, In: *Proc. , European Conference on Composite Materials (ECCM)*, (2014).
49. Soufiane Benaissa, Samir Habibi, Djameleddine Semsoum, Hassen Merzouk, Abdelnou Mezough, Bénali Boutabout, and Alex Montagne, Exploitation of static and dynamic methods for the analysis of the mechanical nanoproperties of polymethylmetacrylate by indentation, *Frattura ed Integrità Strutturale*, (2021), 15(56):46–55.
50. Yves Gaillard and Fabien Amiot, Grid nano-indentation as full-field measurements, *Composites Part A: Applied Science and Manufacturing*, (2020), 132:105807.
51. Daniel P Cole, Todd C Henry, Frank Gardea, and Robert A Haynes, Interphase mechanical behavior of carbon fiber reinforced polymer exposed to cyclic loading, *Composites Science and Technology*, (2017), 151:202–210.
52. Jasper van Meurs, Building a laboratory-scale pultrusion line, (2020).

9 APPENDIX A: PRELIMINARY TESTS

Because pultrusions with Carbon-Elium® have not been performed often yet, a trial production will be done. The goal of this test is to see whether production is even possible on the current set-up and to spot possible problem areas. These test were performed with the first heating section at 90°Celsius and the second heating section at 110°Celsius. These temperatures are based on the research done by Zoller et al. in his paper "Pultrusion of bendable continuous fibers reinforced composites with reactive acrylicthermoplastic elium® resin"[12]. For this test 6 bundles of carbon fiber were used and the speed was increased in steps of 100 mm/min from 200 mm/min to 400 mm/min.

The first test was relatively successful. The production went smooth, without any major issues. Though some points were found which could prove troublesome later on. The first being the pulling force which seemed to increase steadily (figure 59). The first few peaks in this graph are from starting the process, during which the dry fibers are pulled through the die by hand. When solidified product has reached the rollers, the pulling is left to the rollers. This point is seen in the graphs as a sudden decrease in the pulling force. After this a steady increase in the pulling force is seen, most likely caused by a combination of resin sticking to the inside of the die and resin solidification at the die entrance. This could be countered by increasing the pulling speed, as can be seen in the graph, but a different solution would be preferred considering that a higher pulling speed comes with the risk of a decreased polymerization.

A second is resin solidification at the die entrance (figure 60). Some of the resin already starts become solid at the die entrance causing it to stick there. This is expected to be the main reason behind the high pulling forces and can be remedied by increasing the pulling speed, decreasing the temperature or decreasing the air flow at the die entrance.

The last issue found was a small deformation after the pulling rollers (figure 61) at 400 mm/min pulling speed. It is expected that this is caused by an incomplete polymerization although a too high exit temperature could also be the cause. For which exit cooling could be a potential solution.

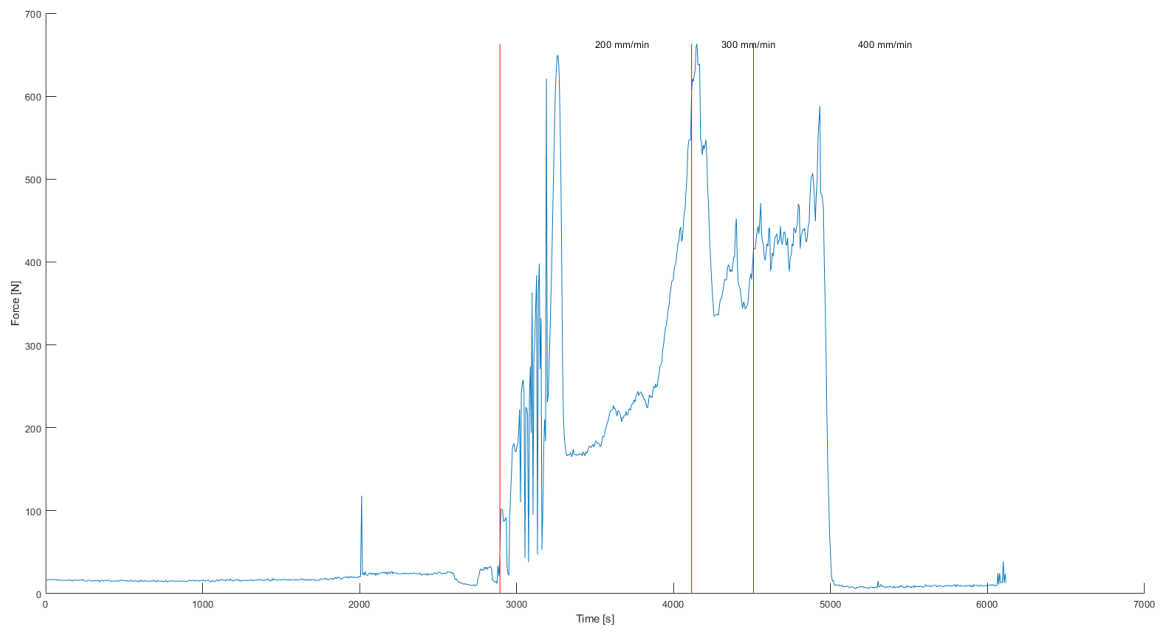


Figure 59: Pulling force during production

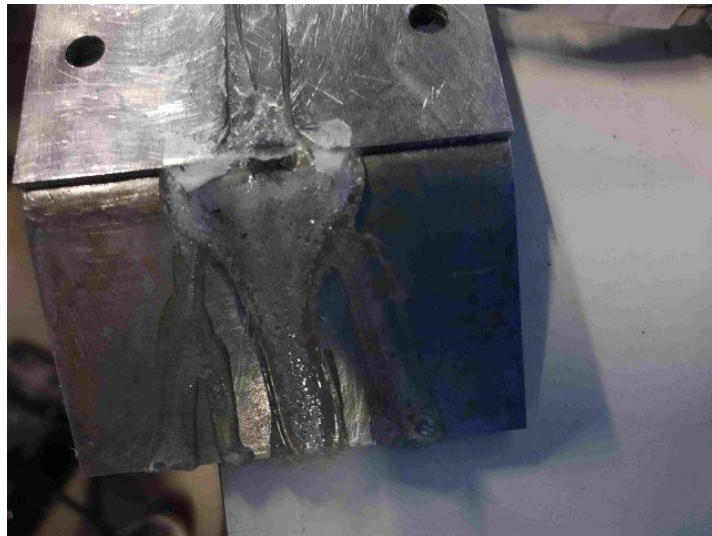


Figure 60: Solidification at die entrance



Figure 61: Deformation at rollers

10 APPENDIX B: HARDNESS FORCE INDENTATION GRAPHS

A few examples of successful and failed indentation will be shown in this section. Including the reasoning for failure.

10.0.a Successful indents

In a successful indent, the indent should be well visible as to know that the location was suitable. The force indentation depth graph should look at least similar to the ones shown below, with a smooth incline a stable pause and a smooth decline. Any strong deviation from this indicates that the indenter hit something other than the resin.

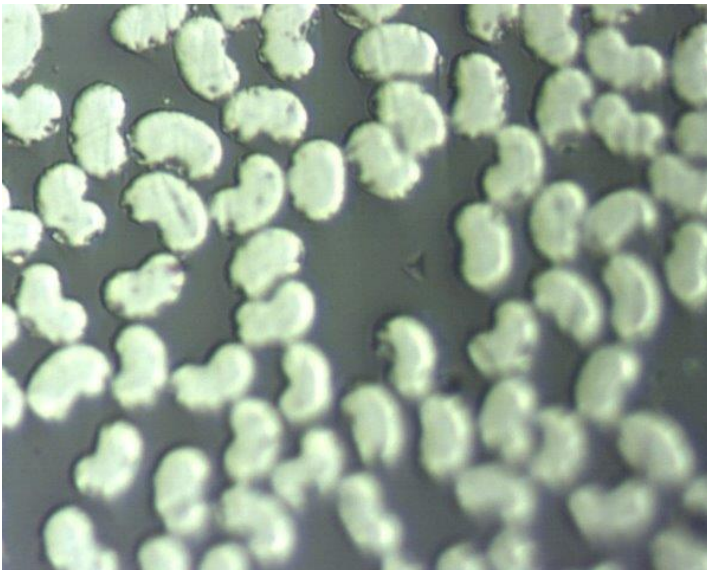


Figure 62: Nano-indentation 100X100 micrometer

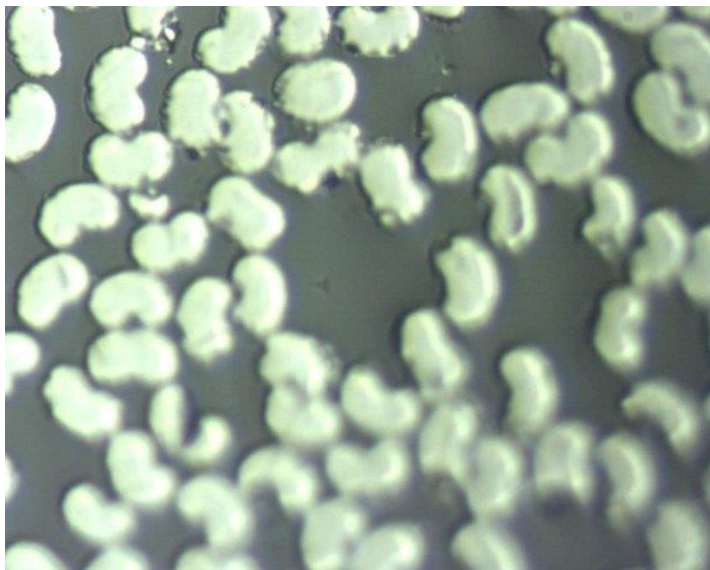
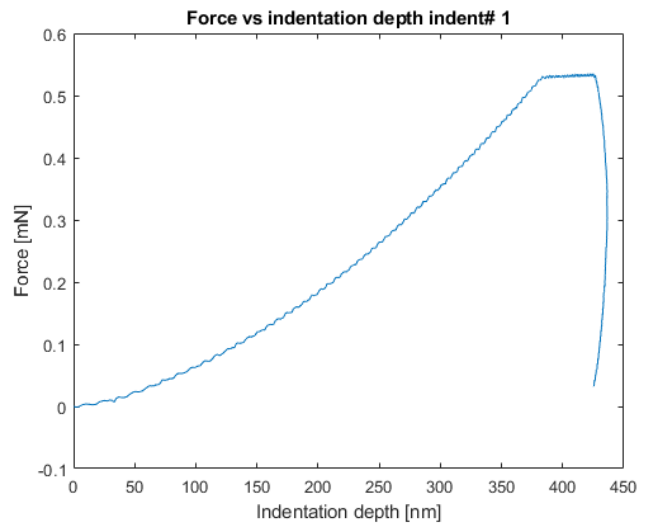
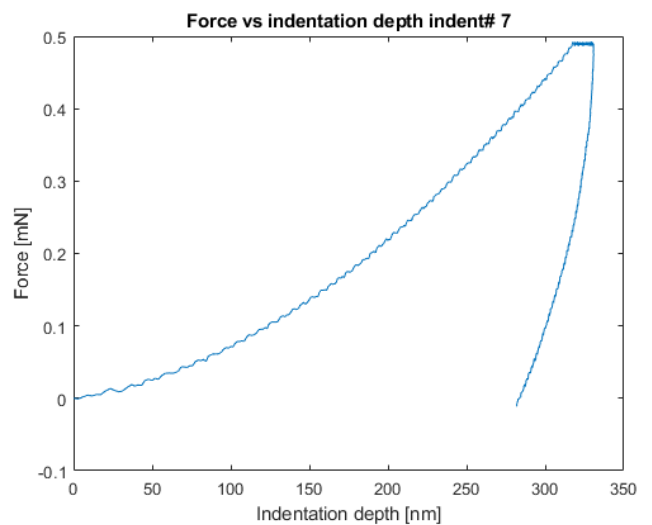


Figure 63: Nano-indentation 100X100 micrometer



Example of a successful indentation with glass fibers. The diameter of the glass fibers is significantly higher and the difference between the fibers and resin is more difficult to see.

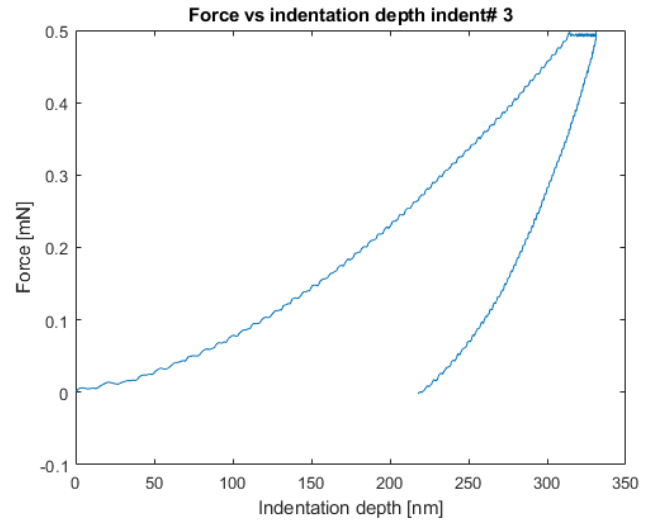
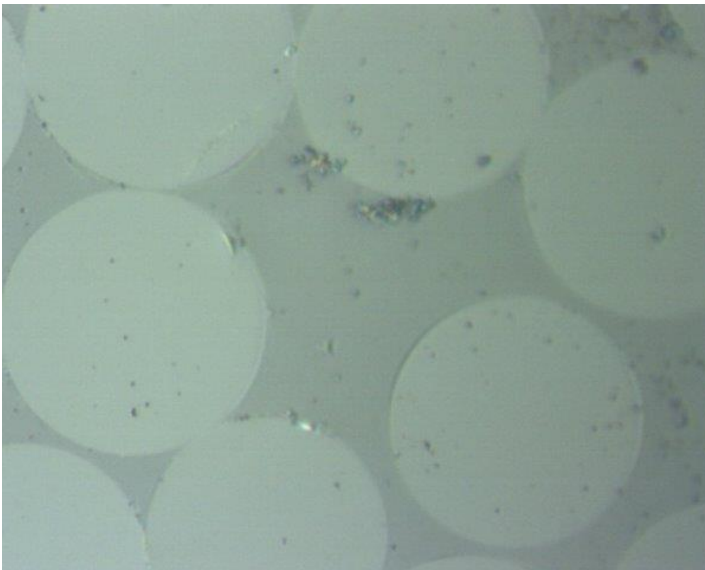


Figure 64: Nano-indentation 100X100 micrometer

10.0.b Failed indents

In this indentation the indent was not visible. The force indentation depth graph also shows a low max depth and the material does not push back during the retrieval of the indenter. This indicates that something other than the polymer was hit during the indentation.

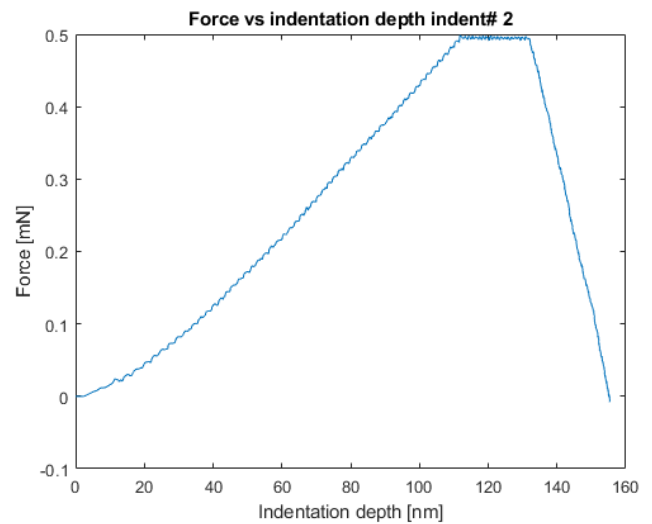
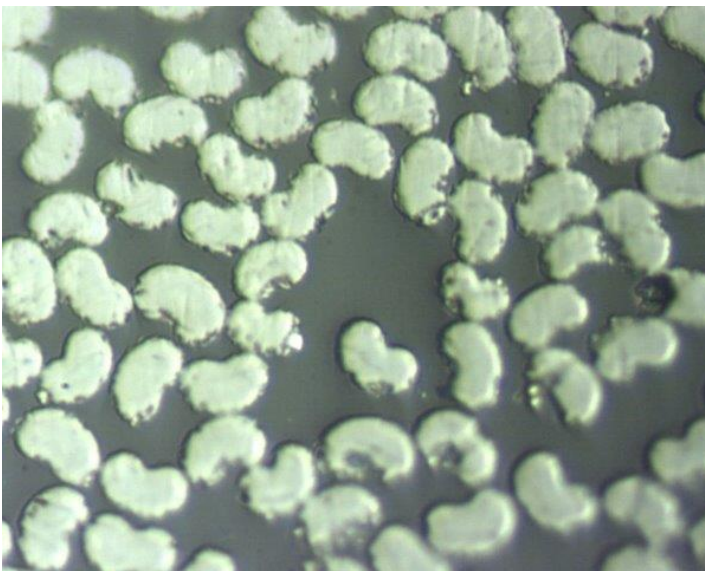


Figure 65: Nano-indentation 100X100 micrometer

On the image a vague indent can be spotted on the left of the resin rich spot very close to a fiber. In the force indentation graph a sudden switch in the incline can be spotted. This indicates a sudden increase in resistance. The indenter first hit the resin and at the depth of roughly 120 nm also hit the fiber causing the sudden increase in resistance.

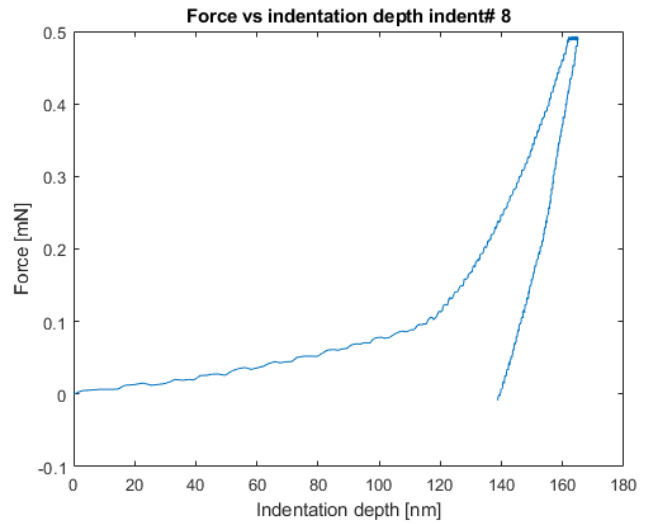


Figure 66: Nano-indentation 100X100 micrometer

No indent was spotted and the max indentation depth is very low. This indicates that a fiber was hit instead of resin.

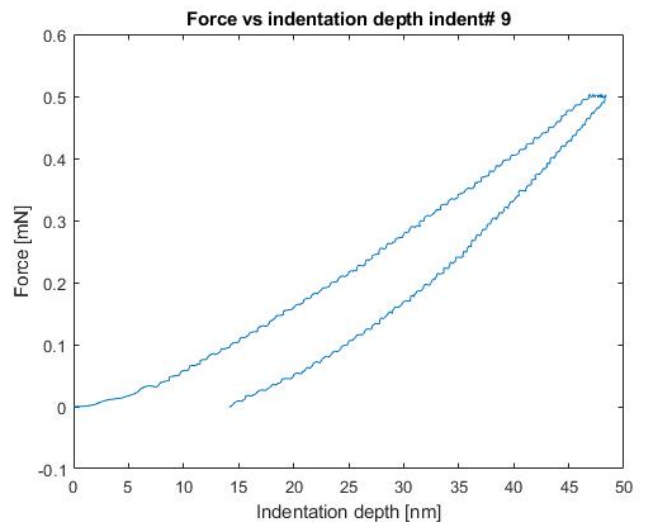
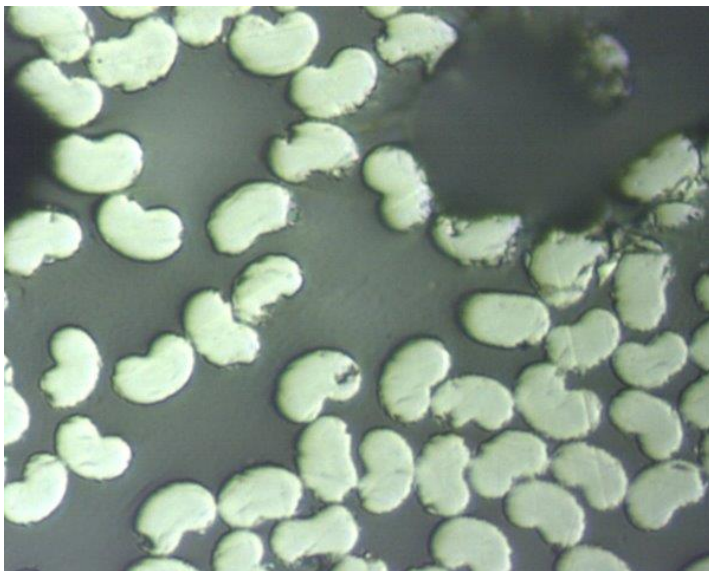


Figure 67: Nano-indentation 100X100 micrometer